NAVAL POSTGRADUATE SCHOOL

MONTEREY, CALIFORNIA

THESIS

DEVELOPMENT OF PHYSICS LECTURE DEMONSTRATIONS FOR UNDERSEA WARFARE

by

Faisal A. Khan

September 2015

Thesis Advisor: Bruce Denardo
Second Reader: Daphne Kapolka

Approved for public release; distribution is unlimited

THIS PAGE INTENTIONALLY LEFT BLANK

REPORT DOCUMENTATION PAGE			Form Approved OMB No. 0704–0188
Public reporting burden for this collection of information is estimated to average 1 hour per response, including the time for reviewing instruction, searching existing data sources, gathering and maintaining the data needed, and completing and reviewing the collection of information. Send comments regarding this burden estimate or any other aspect of this collection of information, including suggestions for reducing this burden, to Washington headquarters Services, Directorate for Information Operations and Reports, 1215 Jefferson Davis Highway, Suite 1204, Arlington, VA 22202-4302, and to the Office of Management and Budget, Paperwork Reduction Project (0704-0188) Washington, DC 20503.			
1. AGENCY USE ONLY ***(Leave blank)***	**2. REPORT DATE** September 2015	**3. REPORT TYPE AND DATES COVERED** Master's thesis	
4. TITLE AND SUBTITLE DEVELOPMENT OF PHYSICS LECTURE DEMONSTRATIONS FOR UNDERSEA WARFARE		**5. FUNDING NUMBERS**	
6. AUTHOR(S) Khan, Faisal A.			
7. PERFORMING ORGANIZATION NAME(S) AND ADDRESS(ES) Naval Postgraduate School Monterey, CA 93943-5000		**8. PERFORMING ORGANIZATION REPORT NUMBER**	
9. SPONSORING /MONITORING AGENCY NAME(S) AND ADDRESS(ES) N/A		**10. SPONSORING / MONITORING AGENCY REPORT NUMBER**	
11. SUPPLEMENTARY NOTES The views expressed in this thesis are those of the author and do not reflect the official policy or position of the Department of Defense or the U.S. Government. IRB Protocol number ____N/A____.			
12a. DISTRIBUTION / AVAILABILITY STATEMENT Approved for public release; distribution is unlimited		**12b. DISTRIBUTION CODE**	

13. ABSTRACT (maximum 200 words)

The importance of educational research is evidenced by many STEM programs (science, technology, engineering, and mathematics), including those by the U.S. Navy. This thesis focuses on the development of new physics lecture demonstrations that are especially relevant for the Undersea Warfare curriculum at the Naval Postgraduate School. Three different phenomena are investigated: (i) reciprocity in linear passive electrical networks, (ii) a Cartesian diver including neutral buoyancy, and (iii) neckless Helmholtz resonators. In (i), we investigate reciprocity in a large two-dimensional resistor grid and a randomly-generated network of resistors, capacitors, and inductors. Reciprocity is important in underwater acoustics transduction. In (ii), we investigate the sinking of a floating body and the instability of a neutrally buoyant body, which are important in the motion of submarines. In (iii), we investigate a resonator consisting of a thin plastic sphere with a hole, and describe an experiment with a precision cylindrical resonator. Helmholtz resonators can be used for the generation of underwater sound, and can unintentionally occur on submarine surfaces. The pursuit of physics demonstrations can contribute to forefront research. In our case, this occurred for the parametric stabilization of a neutrally-buoyant body and for the resonance frequency and quality factor of neckless Helmholtz resonators.

14. SUBJECT TERMS lecture demonstrations, reciprocity, Cartesian diver, neckless Helmholtz resonators			**15. NUMBER OF PAGES** 97
			16. PRICE CODE
17. SECURITY CLASSIFICATION OF REPORT Unclassified	**18. SECURITY CLASSIFICATION OF THIS PAGE** Unclassified	**19. SECURITY CLASSIFICATION OF ABSTRACT** Unclassified	**20. LIMITATION OF ABSTRACT** UU

NSN 7540–01-280-5500 Standard Form 298 (Rev. 2–89)
Prescribed by ANSI Std. 239–18

THIS PAGE INTENTIONALLY LEFT BLANK

Approved for public release; distribution is unlimited

DEVELOPMENT OF PHYSICS LECTURE DEMONSTRATIONS FOR UNDERSEA WARFARE

Faisal A. Khan
Lieutenant Commander, Pakistan Navy
B.E., National University of Sciences and Technology, 2005

Submitted in partial fulfillment of the
requirements for the degree of

MASTER OF SCIENCE IN ENGINEERING ACOUSTICS

from the

NAVAL POSTGRADUATE SCHOOL
September 2015

Approved by: Bruce Denardo
Thesis Advisor

Daphne Kapolka
Second Reader

Daphne Kapolka
Chair, Engineering Acoustics Academic Committee

THIS PAGE INTENTIONALLY LEFT BLANK

ABSTRACT

The importance of educational research is evidenced by many STEM programs (science, technology, engineering, and mathematics), including those by the U.S. Navy. This thesis focuses on the development of new physics lecture demonstrations that are especially relevant for the Undersea Warfare curriculum at the Naval Postgraduate School. Three different phenomena are investigated: (i) reciprocity in linear passive electrical networks, (ii) a Cartesian diver including neutral buoyancy, and (iii) neckless Helmholtz resonators. In (i), we investigate reciprocity in a large two-dimensional resistor grid and a randomly-generated network of resistors, capacitors, and inductors. Reciprocity is important in underwater acoustics transduction. In (ii), we investigate the sinking of a floating body and the instability of a neutrally buoyant body, which are important in the motion of submarines. In (iii), we investigate a resonator consisting of a thin plastic sphere with a hole, and describe an experiment with a precision cylindrical resonator. Helmholtz resonators can be used for the generation of underwater sound, and can unintentionally occur on submarine surfaces. The pursuit of physics demonstrations can contribute to forefront research. In our case, this occurred for the parametric stabilization of a neutrally-buoyant body and for the resonance frequency and quality factor of neckless Helmholtz resonators.

THIS PAGE INTENTIONALLY LEFT BLANK

TABLE OF CONTENTS

THIS PAGE INTENTIONALLY LEFT BLANK

LIST OF FIGURES

LIST OF TABLES

THIS PAGE INTENTIONALLY LEFT BLANK

I. INTRODUCTION

Research in educational physics has been an active field since at least the beginning of the *American Journal of Physics* in 1933, but it is currently even more active due the prevalence STEM programs (science, technology, engineering, and mathematics), including those by the U.S. Navy ("Stem Careers," n.d.). The purpose of this thesis is the development of new physics lecture demonstrations that are especially relevant for the Undersea Warfare curriculum at the Naval Postgraduate School. Physics demonstrations offer a dramatic and tangible means of illustrating concepts which students often have difficulty in understanding.

The thesis involves investigations of demonstrations in three areas: reciprocity in linear passive electrical networks, a Cartesian diver including neutral buoyancy, and neckless Helmholtz resonators. Due to the very different nature of these areas, this thesis is actually three mini-theses. Each topic has its own introduction, body, and conclusions and future work.

Reciprocity in linear passive electrical networks is presented in Chapter II. Reciprocity is important in underwater acoustics for several reasons: It relates transduction coefficients for transducers. It leads to the same directional sensitivity whether a reversible transducer is receiving or transmitting, and it is used in the calibration of a receiving transducer. We investigate a demonstration of reciprocity with an existing large two-dimensional resistor grid. We also describe the development of a randomly-generated network of resistors, capacitors, and inductors as a demonstration of reciprocity, and computer simulations are done.

A Cartesian diver including neutral buoyancy is presented in Chapter III. An understanding of the sinking and rising of a Cartesian diver leads to an explanation of one way that submarines sink or rise. In addition, a different perspective on our Cartesian diver demonstration leads to an explanation of how

scuba divers and most fish sink or rise. Neutral buoyancy can also be demonstrated, although the equilibrium is unstable, and we describe how this can be clearly demonstrated. A hydrostatic paradox of the instability arises for an incompressible liquid in a rigid container. We explicitly show how the paradox is resolved when the container has nonzero compliance. We also develop a theory for the parametric stabilization of neutrally-buoyant body.

Research on neckless Helmholtz resonators is presented in Chapter IV. Helmholtz resonances occur in variety of systems, including underwater sound. Resonances can be intentional, as in low-frequency projectors, or unintentional and unwanted, as in surfaces of submarines. We present a quantitative lecture demonstration of a thin plastic sphere with a hole. Without inclusion of the end correction in the theory, the predicted resonance frequency is more than three times greater than the observed frequency. Inclusion of the end correction reduces the error, but we show in an experiment that the deviation is still substantially outside the error bars. We present the results of an experiment with a precision cylindrical resonator in order to carefully compare theory and experiment for a neckless Helmholtz resonator. In addition to the educational importance of new physics demonstrations, efforts in this area can contribute to forefront research. An example is a water wave analog of the Casimir effect (Denardo et al., 2009), which was recently cited in an article on the foundations of quantum mechanics (Bush, 2015). In this thesis, two contributions to forefront research arise: the parametric stabilization of a neutrally-buoyant body, and the resonance frequency and quality factor of neckless Helmholtz resonators.

II. RECIPROCITY IN ELECTRICAL NETWORKS

A. INTRODUCTION

A very large variety of physical systems that involve an external drive and a response exhibit a remarkable property called *reciprocity*. The system must be *linear*. For example, if the drive is doubled, the response is doubled. For a general although necessarily imprecise statement of reciprocity, consider a system that is driven at any point 1 and the response is measured at any other point 2. The *transfer impedance* is defined as Z_{12} = drive$_1$/response$_2$. Consider switching the drive and response points. Reciprocity is simply that *the transfer impedance is symmetric*: $Z_{12} = Z_{21}$. In particular, if the drive is the *same* at the two points, reciprocity means that *the same response occurs if the driver and receiver are interchanged.*

Precise definitions of the drive and response vary among systems. Reciprocity only holds for certain *conjugate* variables. For oscillatory mechanical systems, the drive is the force and the response is the velocity, or the velocity is drive and force is the response. For electrical circuits, the drive is the voltage and the response is the current, or the current is the drive and the voltage is the response.

Reciprocity is important in the case of reversible transducers for several reasons. It relates the transduction coefficients that dictate the conversion of energy from electrical to mechanical and from mechanical to electrical. It also leads to a simple relationship between the receiving sensitivity and transmitting response, so that the directional pattern is the same whether the transducer is used as a receiver or transmitter. Hence, the receiving characteristics can be determined from transmission measurements, or vice versa. Still another role occurs in the absolute far-field calibration of a receiving transducer, which can remarkably be accomplished with only a reciprocal transducer and a transmitter,

where the receiving and transmitting responses of the latter transducers need not be known (Kinsler et al., 2000).

Reciprocity is well-known to hold for any passive electrical network with linear elements (Wilson, 1989). Refer to figure1. The voltage sources can be AC or DC. If they are ac, they must have the same frequency. Electrical network reciprocity (symmetry of the transfer impedance) means the following:

$$\left.\frac{V_j}{I_k}\right|_{V_k=0} = \left.\frac{V_k}{I_j}\right|_{V_j=0} .$$

Note that the response current refers to a closed circuit (zero voltage across the terminals). The drive voltage will cause a current dictated by Kirchhoff's laws.

Figure 1. Reciprocity in an arbitrary linear electrical network

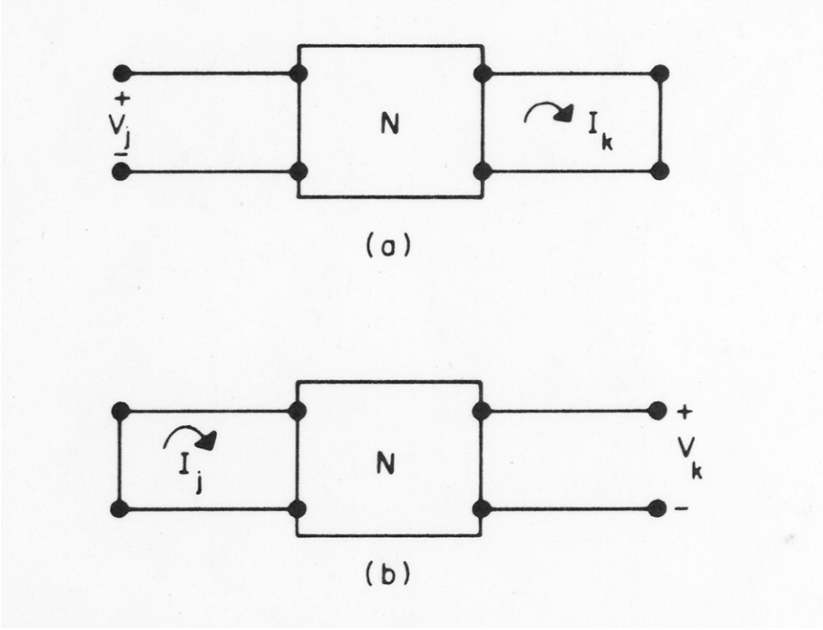

Shown are two arbitrary pairs of nodes of the network. Reciprocity means that the transfer impedance is symmetric; that is, Vj/Ik equals Vk/Ij. From O. B. Wilson, 1989, *Introduction to theory and design of sonar transducers*, Peninsula Publishing, Los Altos, California, Ch. 2.

We have not yet found a general proof, so demonstrations are especially important.

An electromechanical system transducer may or may not obey reciprocity. It can be shown (Denardo, 2015) that a transducer is reciprocal (i.e., obeys reciprocity) if the transduction coefficients are *equal*. The importance of this is that an equivalent electrical circuit exists, and that therefore that Kirchhoff's laws apply. If the transduction coefficients are *not* equal, then an equivalent electrical circuit does *not* exist. Fortunately, nearly all sonar transducers are reciprocal.

In Section B, we investigate a demonstration with a large two-dimensional grid of approximately identical resistors. In Section C, we consider a more general system of a randomly-generated linear electrical network of resistors, capacitors, and inductors. In Section D, reciprocity of the randomly-generated network is verified with the electrical circuit software Pspice. Conclusions and future work are presented in Section E.

B. LARGE TWO-DIMENSIONAL RESISTOR GRID

In the late 1990s, a large two-dimensional resistor grid was added to the Physics Lecture Demonstration Laboratory (Figure 2). The grid is a 12 by 12 array of 1.00 $\mathrm{k}\Omega$ resistors that are connected at the 13 by 13 nodes. As explained by Denardo et al. (1999), the main purpose of the grid is to approximate an infinite two-dimensional grid of identical resistors with resistance R0, which offers a classic problem in equivalent resistance: What is the resistance across two adjacent nodes? The answer, which can be obtained simply by the principle of superposition, is R0/2. The equivalent resistance across other nodes can be only determined with substantial effort, which is indicated by the remarkable fact that the equivalent resistance for an elementary diagonal is $2R0/\pi$, which includes a factor of π! The apparatus is useful as a lecture demonstration to approximately confirm the theoretical predictions, and it can also be used in an educational laboratory.

Figure 2. A 12 by 12 grid of identical resistors with resistance 1.00 kΩ

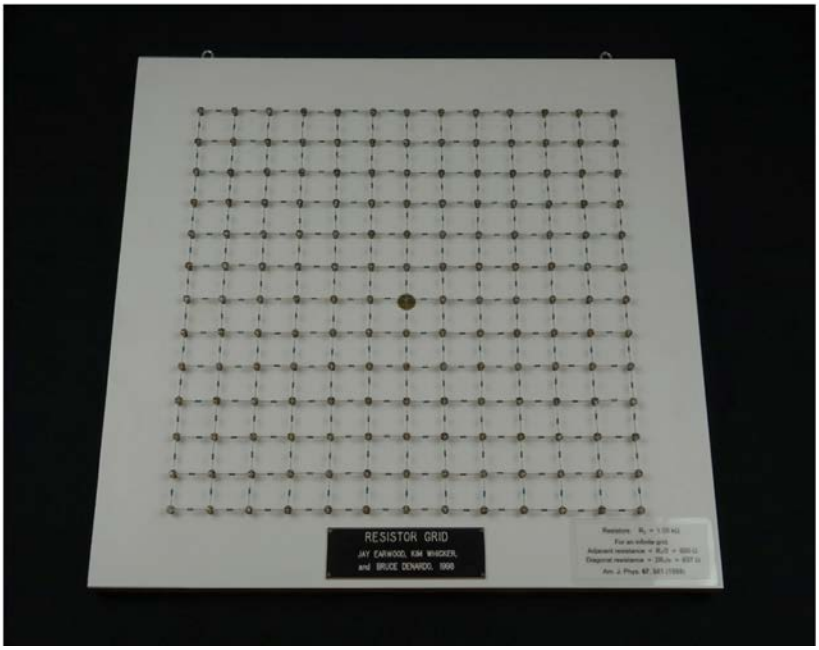

A 12 by 12 grid of identical resistors with resistance 1.00 kΩ. The overall dimensions of the apparatus are 24 inches by 24 inches by 3/4 inch.

While beginning to work on this thesis, we realized that the two-dimensional resistor grid could be useful as a demonstration of reciprocity. The idea is simple. Select any pair of nodes and connect a dc voltage source across it. Measure the current between any other pair of nodes. It is important to note that, according to reciprocity for electrical networks, this pair of nodes must be shorted and the current measured through the short. That is, an ideal current meter should simply be connected between the terminals. Reciprocity predicts that, if the constant voltage source and the current meter are interchanged, the same current should occur. To describe the terminals, we label the nodes of the grid with the indices shown in Figure 3.

Figure 3. Labeling of nodes of the two-dimensional grid of identical resistors

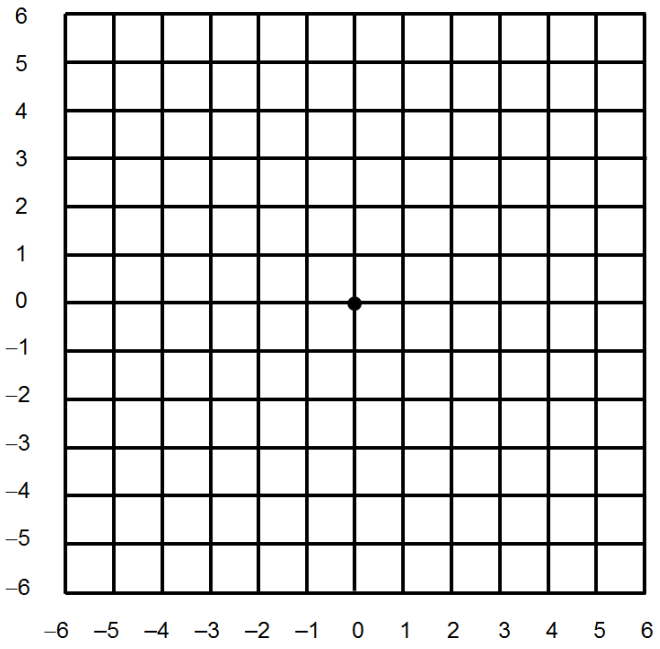

Labeling of nodes of the two-dimensional grid of identical resistors. Each unit line segment represents a resistor. The numbers denote the x and y indices of the nodes. The dot denotes the origin.

To make the demonstration dramatic, two highly asymmetric pairs of terminals can be selected. An example is shown in Figure 4. One pair of terminals is (–6, 6) and (6, –6), while the other pair of terminals is (–1, 1) and (1, –1). As stated above, reciprocity predicts the currents are *identical* when the source is switched from one pair of terminals to the other. To qualitatively appreciate this fact, note that the currents in the two drive-and-response cases both tend to be small for the following reasons. When the voltage source is across the outer terminals, the current across the inner pair tends to be small because the equivalent input resistance is large. When the voltage source is across the inner pair of terminals, the equivalent input resistance is small, but the voltage and thus current across the outer pair of terminals will tend to be small because the current distribution is localized to the vicinity of the inner pair.

Figure 4. Demonstration of reciprocity with the large two-dimensional resistor grid

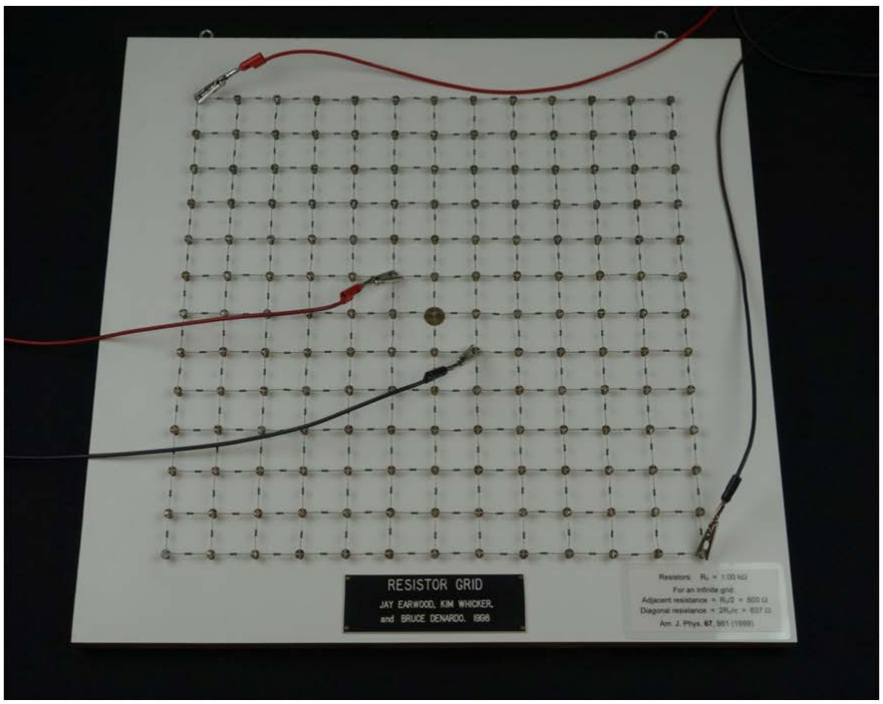

Demonstration of reciprocity with the large two-dimensional resistor grid. A constant dc voltage source is connected across the outer pair of terminals, and the current is measured across the inner pair. The drive and response wire leads are then interchanged. Reciprocity predicts that the currents are the same.

We used precision equipment to perform the measurements (HP E3615A DC power supply and HP 34401A multimeter). The resistors have a maximum power of 1/8 W. The drive voltage needs to be as large possible because the currents can be small. The greatest current will occur when the source is applied across two adjacent nodes. A drive voltage of 10.00 V_{dc} will dissipate the power $V^2/R = 10^2/10^3 = 1/10$ W in the resistor between the nodes, which should not cause the resistor to overheat. We thus use 10.00 V_{dc} as our drive voltage.

The results of the measurements are shown in Table 1, where we have included two additional pairs of terminals. The percentage difference between all pairs of currents is small (less than 1%) over a broad range of two orders of magnitude. We originally used a later-model multimeter (Agilent 34410A), but we

found roughly *twice* the percentage deviation, because the shunt resistance is 2 Ω for the Agilent meter and 5 Ω for the HP meter. We believe that the Agilent meter is faulty, because it is substantially inconsistent with our experimentation involving the shunt resistance (explained below).

Table 1. Experimental results for the two-dimensional resistor grid

drive terminals	response terminals	response current (mA)	percentage deviation
(–6, –6) and (6, 6)	(–1, –1) and (1, 1)	0.927	0.4%
(–1, –1) and (1, 1)	(–6, –6) and (6, 6)	0.931	
(4, 4) and (6, 6)	(–1, –1) and (1, 1)	0.0437	0.2%
(–1, –1) and (1, 1)	(4, 4) and (6, 6)	0.0438	
(0, 0) and (6, 0)	(0, 0) and (1, 0)	5.157	0.8%
(0, 0) and (1, 0)	(0, 0) and (6, 0)	5.197	

Experimental results for the two-dimensional resistor grid. The drive voltage is 10.00 V_{dc} in all cases. Reciprocity is confirmed to an accuracy of better than 1%.

Reciprocity appears to be confirmed in Table 1, but are the deviations within experimental error? Reciprocity predicts that the currents in each set of pairs of terminals are identical, *regardless* of whether the resistors are identical or not. The fact that the currents are not exactly the same within the accuracy of the measurement equipment is thus *not* due to deviations of the resistances. The deviations must be due to the measurement equipment, which we now consider.

The data in Table 1 were taken with banana wire leads of nominal length 3 feet, which have a resistance of about 0.01 Ω. Because this value is very much smaller than the typical 1.0 kΩ resistance of the grid, we expect that the effect of the wire leads on the measurements is negligible. We confirmed this by first retaking the data with drive leads of nominal length 6 feet (twice the original length), which have a resistance of about 0.03 Ω. There was either no change or

very little change in the data. We then retook the data with response leads of length 6 feet. There was again either no change or very little change in the data.

The deviations of the response currents in Table 1 should not be due to the DC power supply, because it maintains a constant 10.00 V potential difference regardless of what pair of terminals are driven. The *current* that it delivers will depend upon the pair, but the voltage should not. We directly verified that the voltage across the pairs of terminals is constant to a high degree of accuracy (less than one part in 10^5).

We are thus finally led to the current meter. By reciprocity, the current through a short between a pair of response terminals must be exactly the *same* when the drive and response are interchanged. However, the current distributions in the grid are not in general the same in both cases. How can the connection of an actual current meter yield small but significantly *different* readings when the drive and response are interchanged? Due to the shunt resistance of the current meter, the terminals are *not* being exactly shorted, which alters the current distribution in the network including the current across the terminals. In general, this alteration will be *different* when the drive and response are interchanged.

The shunt resistance for the multimeter acting as a current meter in our case is specified as 5 Ω, which is 0.5% of our characteristic resistance of 1.0 kΩ in the resistor grid. We thus expect deviations on the order of 0.5% in our reciprocity measurements, which is what we observe (Table 1). This suggests that we have confirmed reciprocity within the experimental error of our apparatus. This result is expected to be somewhat coincidental due to the uncertainty in the actual resistance of each of the resistors. However, the idea that the shunt resistance is responsible for the deviations can be directly tested. We connected the wire leads for the response measurement to a dual banana plug connector with a 1 Ω resistor across it to act as a shunt resistance, and used the multimeter as a voltage meter. Due to the high impedance of the voltmeter, the

voltage across the connector is proportional to the current to the shunt resistor. For the cases in Table B.1, the percentage deviations of the voltages for each of the three sets of reciprocity cases were roughly reduced from 0.5% to 0.1%, which is just what is expected for a reduction of the shunt resistance from 5 Ω to 1 Ω.

In performing a lecture demonstration with the large two-dimensional grid of resistors, the pairs of terminals can be *randomly* selected, which may offer a more convincing and dramatic example of reciprocity. One way to accomplish this is with four colored dice in the following manner. The colors must all be different. One color is designated to be the absolute value of x-index in Figure 3, and one color is designated to be the sign of the index, where an even value corresponds to a positive value and an odd value corresponds to the negative value. The two other colors are similarly associated with the y-index. A rolling of the four dice randomly yields one terminal, although the axes (a zero index) are excluded. If the terminals are the same, the dice must be rolled again. Four rollings of the dice yield two random pairs of terminals. If the pairs are identical, an additional rolling of the dice is required.

C. RANDOMLY GENERATED LINEAR ELECTRICAL NETWORK

For a more general demonstration of electrical network reciprocity than in section B, we consider an actual electric circuit consisting of resistors, capacitors, and inductors, where the values of the elements of each type are the same:

$$R = 1.0\ \mathrm{k}\Omega \qquad C = 1.0\ \mathrm{nF}, \qquad L = 1.0\ \mathrm{mH}. \qquad \text{(C.1)}$$

The drive parameters are chosen to be 10 V_p at 100 kHz, although we will also investigate a broad range of amplitudes and frequencies (Section E). We choose a total of 6 terminals in a 2 by 3 array on a board that has rough dimensions of 9 by 12 inches (Figure 5). The terminals are binding posts with banana plug connections. It may be advisable to make the connections of the

circuit elements with eyelets rather than solder, so that they can be readily changed if necessary.

Figure 5. Layout of terminals for random electrical linear network of resistors, capacitors, and inductors

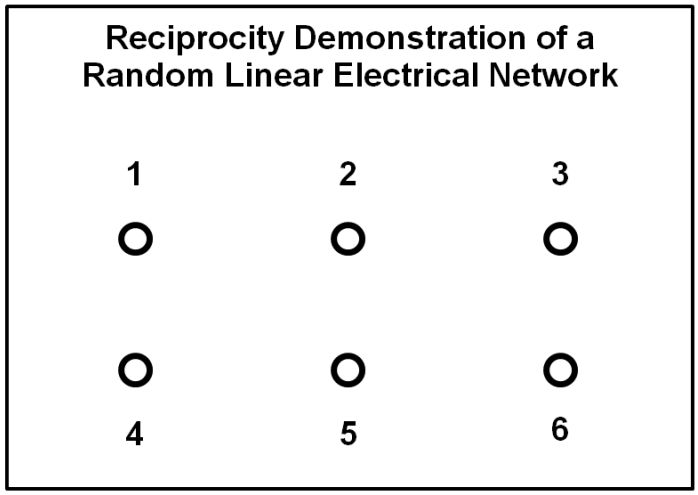

Layout of terminals for random electrical linear network of resistors, capacitors, and inductors. The specific elements and their corresponding pairs of terminals are chosen by successively rolling 3 dice.

To emphasize the generality of reciprocity here, we consider a *random* electrical network. We generate this network by successively rolling three dice. A designated dice yields the circuit element, where 1 or 4 refers to a resistor R, 2 or 5 to a capacitor C, and 3 or 6 to an inductor L. The other two dice yield the pair of terminals across which the circuit element is connected. If the two dice have the same value, they are rolled again. If any duplications of the circuit element and the pair terminals occur, they are neglected. Otherwise, the circuit may be become too cluttered. The process is continued until the circuit is deemed to have a sufficient number of circuit elements. In view of the predicted reciprocity, the natural criterion for a sufficient number of elements is that a drive voltage

across any pair of terminals yields a *nonzero* current through a short across any other pair of terminals. We ensure this criterion by connecting an ac voltage source across each pair of terminals, and checking that the current delivered by the source is not zero. If all of the values are nonzero, then the criterion is met. Note that 5 + 4 + 3 + 2 + 1 = 15 measurements are required. A result of successive rollings of the dice yielding 20 distinct electrical connections is shown in Table 2.

Table 2. Circuit elements and corresponding terminals of a randomly-generated electrical 6-terminal network

number:	1	2	3	4	5	6	7	8	9	10
element:	R	R	C	L	C	R	L	C	L	L
terminals:	3 4	4 5	1 4	1 5	2 4	2 3	2 6	3 4	2 3	3 6

number:	11	12	13	14	15	16	17	18	19	20
element:	L	C	R	L	R	L	C	R	L	C
terminals:	1 3	3 5	1 2	2 5	1 6	1 2	1 3	1 3	5 6	1 6

Circuit elements and corresponding terminals of a randomly-generated electrical 6-terminal network, where R denotes a resistor, C denotes a capacitor, and L denotes an inductor. The random generation was accomplished by successively rolling 3 dice.

The system should be constructed first with electrical circuit software, adding one circuit element at a time and checking for ac continuity between every pair of terminals. Once full continuity has been achieved, the construction can stop. The software should also be used to check reciprocity, including the phase and the issue of different possible variables in the transfer impedance.

In a demonstration, the drive voltage from a function generator is applied across an arbitrary pair of terminals, and another arbitrary pair of terminals is chosen to be the response terminals. The two pairs of terminals are chosen by rolling 2 pairs of distinctly different dice. Note that it is permissible for two pairs of terminals to share one terminal (but not both). For the purposes of a computer experiment of the reciprocity in the next section, a set of values corresponding to the rolling of the dice is shown in Table 3.

Table 3. Pairs of random terminals for the purpose of verifying reciprocity

test case:	1		2		3	
pairs of terminals:	4, 5	1, 4	1, 3	3, 6	4, 6	1, 2

Pairs of random terminals for the purpose of verifying reciprocity. The pairs were generated by rolling two distinct pairs of dice.

In a lecture demonstration, a proper verification of reciprocity would include both the amplitude and phase of the current. To do this, it is best *not* to directly measure the amplitude of the current with a current meter connected across the response terminals. Rather, a small resistor is added in series with the short across the response terminals, and the voltage across the series resistor is displayed with the drive voltage on an oscilloscope. The series resistor will alter the amplitude and phase of the current by a small amount as demonstrated in Section B. The amplitude of the current is proportional to the amplitude of the response voltage, and the phase of the current relative to the drive voltage is the same as the phase of the response voltage.

In a lecture demonstration, the values of amplitude and relative phase of the response voltage are written on the blackboard. The drive and response

terminals are then interchanged, and the values of the amplitude and relative phase are compared to the original values. According to reciprocity, they should be the same!

However, there is a problem. The phase of the response depends upon the choice of the positive and negative terminals of the drive as well as the response. By switching either one of these, a 180^o phase shift is introduced in the response. Hence, we can only expect the phase of the two responses to agree within $\pm 180^o$.

We have considered the classic case of a drive voltage V_1 across any pair of terminals and a response current I_2 through a short across any other pair of terminals. Reciprocity is that the transfer impedance $Z_{12} = V_1/I_2$ is symmetric. But there are *three* other possibilities. One is a drive current I_1 through a short between any pair of terminals, and the response voltage V_2 across any other pair of terminals. The transfer function is I_1/V_2. The symmetry of the transfer impedance Z_{12} does *not* imply that reciprocity will also hold in this case and yet it is known to hold. The current distributions are *not* the same, because current flows from the drive voltage, but current does not flow in the case of the response voltage. Nevertheless, as mentioned in section A, it is known that reciprocity also holds in this case. A third possibility is a drive voltage V_1 across any pair of terminals and a response voltage V_2 across any other pair of terminals. The transfer function is V_1/V_2. The final (fourth) possibility is a drive current I_1 through a short across any pair of terminals and a response current I_2 across any other pair of terminals. The transfer function is I_1/I_2. Reciprocity does not hold for the latter two possibilities. Note that the apparatus could be used to show that reciprocity holds for a drive current and voltage response, but does not hold in the unmixed voltage and unmixed current cases.

D. COMPUTER SIMULATIONS OF RANDOM ELECTRICAL NETWORKS

Computer simulations of electrical circuits are commonly done with PSpice software (Vladimirscu, 1994). We used the student version, which can be downloaded free online. System elements were added while checking for AC continuity between each pair of terminals. Firstly, a circuit of 10 elements was constructed, which was followed by construction of a circuit with 20 elements. After achieving complete AC continuity (refer to Section C), reciprocity tests were conducted. A drive voltage was applied across a pair of arbitrary terminals, while the response current through a short between another arbitrary pair of terminals was measured. For the purpose of generality, both the drive voltage and response current pairs of terminals were randomly chosen by rolling a pair of dice twice.

Certain problems were encountered while constructing the circuit in PSpice software. Firstly, in order to have current passing through an inductor, a small amount of resistance was required to be added in series with each inductor element. This additional resistance had no effect on the actual functioning of circuit, but was actually required due to a PSpice software limitation. The output had no effect whether this additional resistance was kept as $1.0 \times 10^{-3}\ \Omega$ or $1.0 \times 10^{-7}\ \Omega$. Secondly, to measure the current across a pair of arbitrary response terminals, terminals were required to be shorted with an ammeter in series. To achieve this in PSpice software, a small amount of resistance was added in series with the short and the current was measured through this added resistance. Current was measured with the current marker available in PSpice instead of a regular ammeter. This additional resistance had no effect on the actual functioning of circuit, but was required due the PSpice software limitation. Again, the output had no effect whether this additional resistance was kept as $1.0 \times 10^{-3}\ \Omega$ or $1.0 \times 10^{-7}\ \Omega$.

1. 10-Element Network

A peak drive voltage of 10 V with a frequency of 100 KHz was applied across an arbitrary pair of terminals. The magnitude and phase of the current through a short across another arbitrary pair of terminals were measured using a frequency sweep across a broad range of frequencies. The circuit with drive voltage applied across the pair (1, 2) and response current across the pair (4, 6) is shown in Figure 6 (top). The resultant output of the current magnitude and phase across the response terminals is shown in Figure 6 (middle and bottom).

To prove reciprocity, we switch the drive and response. That is, the drive voltage is now applied across the pair (4, 6) and the response current is across pair (1, 2), as shown in Figure 7 (top). The output with an AC sweep showing current amplitude and phase across response terminals is shown in Figure 7 (middle and bottom). The amplitudes agree within the precisions of Pspice, which is one part in 10^5. The phases similarly agree, although it should be noted that we chose the polarity of the current meter such that there was not a $\pm 180^o$ phase difference (refer to Section C) with the phase in Figure 6 (bottom).

Figure 6. Ten element network with drive voltage across the pair (1, 2) and current response across the pair (4, 6)

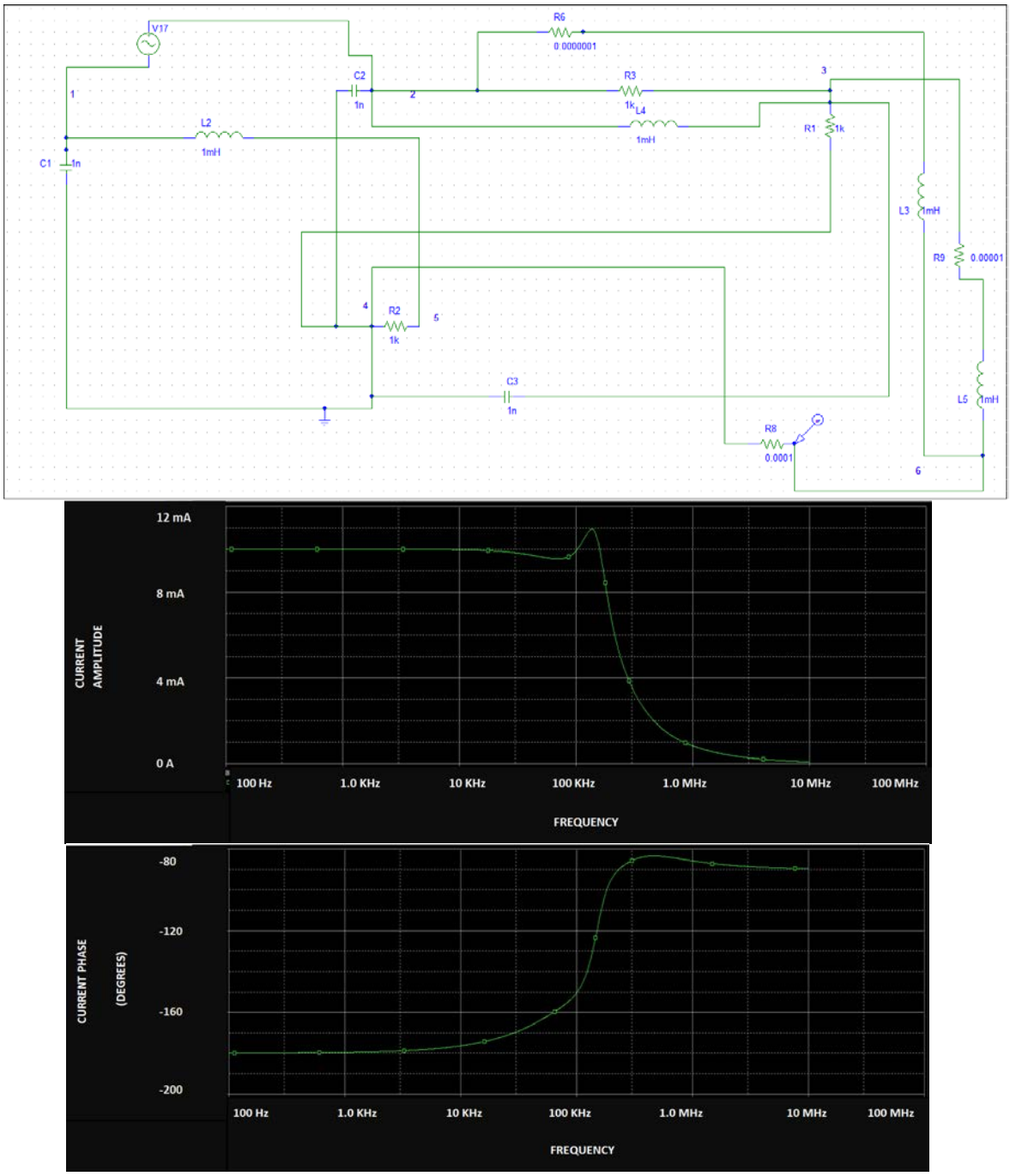

10-element network with drive voltage across the pair (1, 2) and current response across the pair (4, 6). The top figure shows the circuit. The two graphs are the current amplitude and phase for a drive frequency sweep from 0.1 kHz to 100 MHz with a constant voltage amplitude of 10 V.

Figure 7. Ten element circuit with drive voltage across the pair (4, 6) and response current across the pair (1, 2)

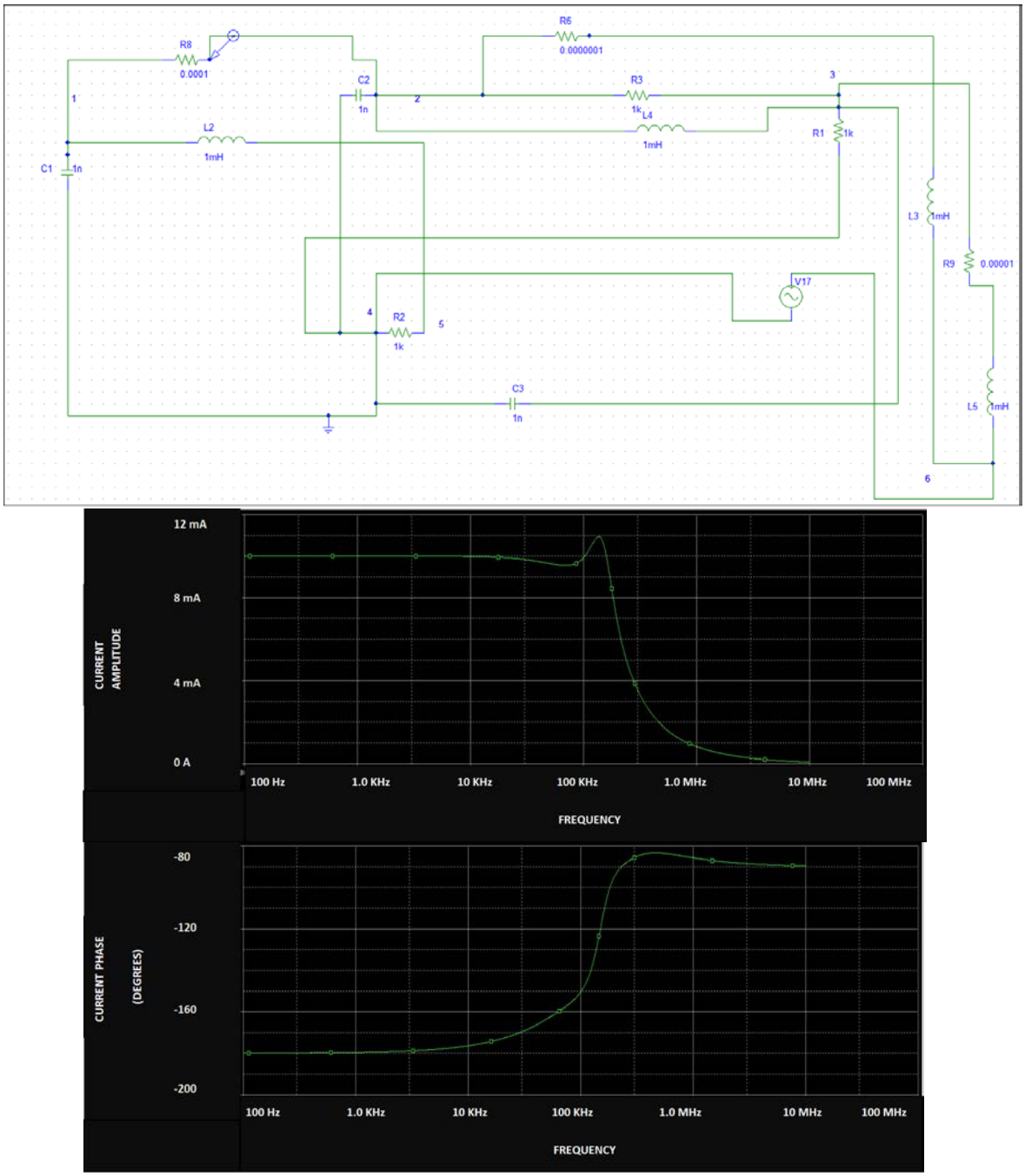

10-element circuit with drive voltage across the pair (4, 6) and response current across the pair (1, 2). Compared to Fig. E.1, the drive and response terminals have been interchanged.

Values of current amplitude and phase for different random combinations of drive and response terminals are given in Table 4. The values are for current magnitude and phase measured at 100 kHz. The current magnitude and phase values are equal to the 5 significant figure precision of Pspice.when drive and response terminals are interchanged. This is remarkable in view of all the calculations that are done in the software.

Table 4. Response current amplitude and phase for drive voltage 10 V and drive frequency 100 kHz

drive terminals	response terminals	current amplitude (mA)	current phase (deg)
(1, 4)	(4, 5)	15.916	90.000
(4, 5)	(1, 4)	15.916	90.000
(1, 3)	(3, 6)	1.1387	-40.999
(3, 6)	(1, 3)	1.1387	-40.999
(1, 2)	(4, 6)	9.958	-149.990
(4, 6)	(1, 2)	9.958	-149.990

We also wanted to check the linearity of reciprocity. Table 5 shows results for terminals (1, 2) and (4, 6) in Table 4, but with drive amplitudes that vary by three orders of magnitude. Reciprocity in both amplitude and phase is again verified to the precision of PSpice.

Table 5. Response current amplitude and phase for different drive voltages and drive frequency 100 kHz

peak drive voltage (V)	drive terminals	response terminals	current amplitude (mA)	current phase (deg)
1	(1, 2)	(4, 6)	0.9958	-149.990
1	(4, 6)	(1, 2)	0.9958	-149.990
10	(1, 2)	(4, 6)	9.958	-149.990
10	(4, 6)	(1, 2)	9.958	-149.990
100	(1, 2)	(4, 6)	99.581	-149.990
100	(4, 6)	(1, 2)	99.581	-149.990
1000	(1, 2)	(4, 6)	995.8	-149.990
1000	(4, 6)	(1, 2)	995.8	-149.990

2. 20-Element Network

To more fully test for reciprocity, we considered a random 20-element electrical network as described in Sec. C. The circuit with drive voltage applied across the pair (1, 2) and response current across the pair (3, 4) is shown in Figure 8 (top). The output due to an AC sweep showing current magnitude and phase across the response terminals is shown in Figure 8 (middle and bottom).

To examine reciprocity, we constructed the circuit with the drive voltage across pair (3, 4) and the response across pair (1, 2). The circuit is shown in Figure 9 (top). The output for an AC sweep showing the current magnitude and phase across the response terminals is shown in Figure 9 (middle and bottom). The current magnitude and phase results matched to 5 significant figures, just as in the case of the random 10-element network.

From above results, it is clear that reciprocity holds for random systems with 10 and 20 elements. The same can be proved by construction of a physical circuit for a lecture demonstration, although the physical circuits are expected to show some deviation from these exact values, due to the aforementioned problem with the nonzero impedance of the ammeter. We leave this for future work.

Figure 8. Twenty element network with drive voltage across the pair (1, 2) and current response across the pair (3,4)

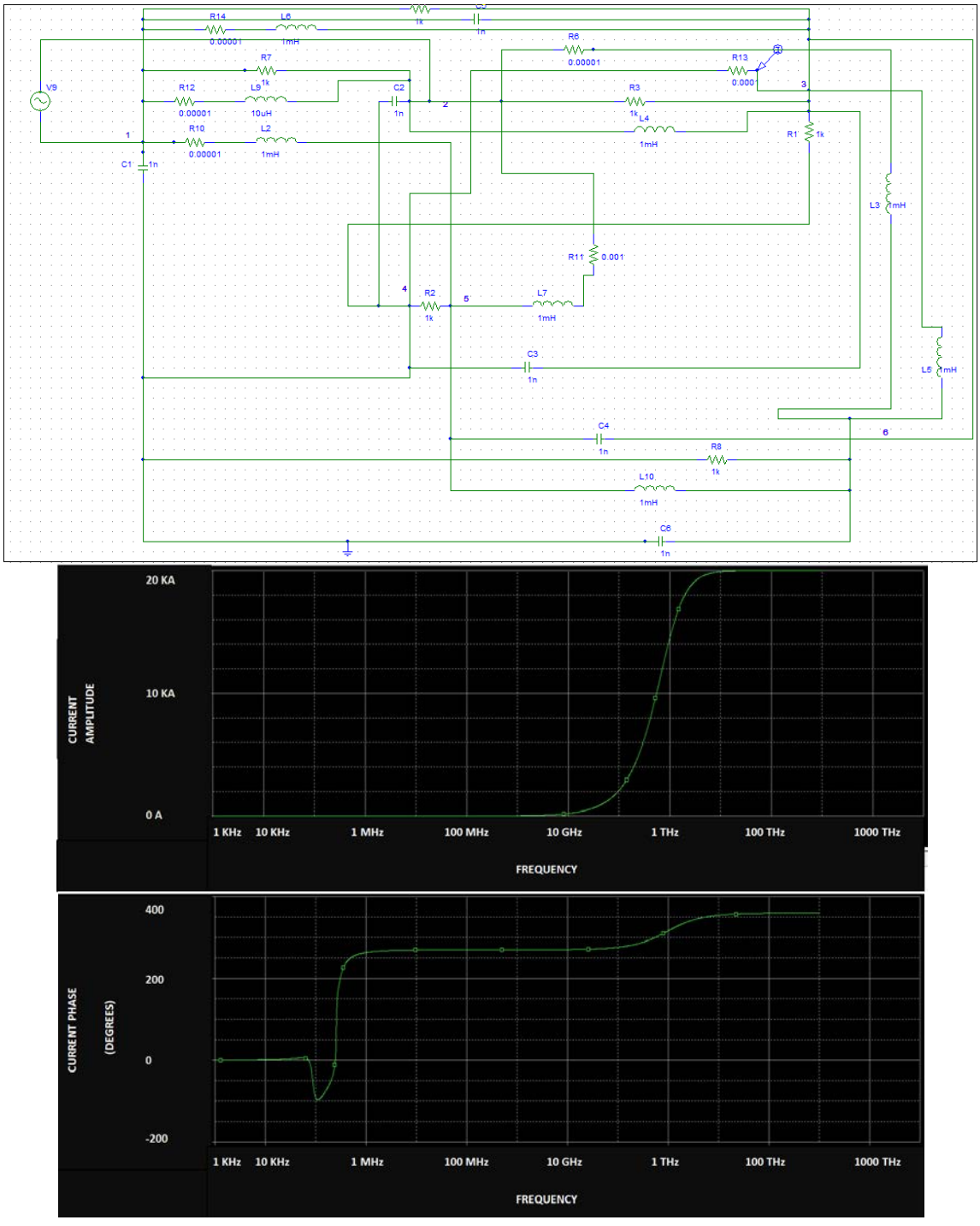

20-element network with drive voltage across the pair (1, 2) and current response across the pair (3, 4). The top figure shows the circuit. The two graphs are the current amplitude and phase for a drive frequency sweep from 1 kHz to 1000 THz with a constant voltage amplitude of 10 V.

Figure 9. Twenty element circuit with drive voltage across the pair (3,4) and response current across the pair (1, 2)

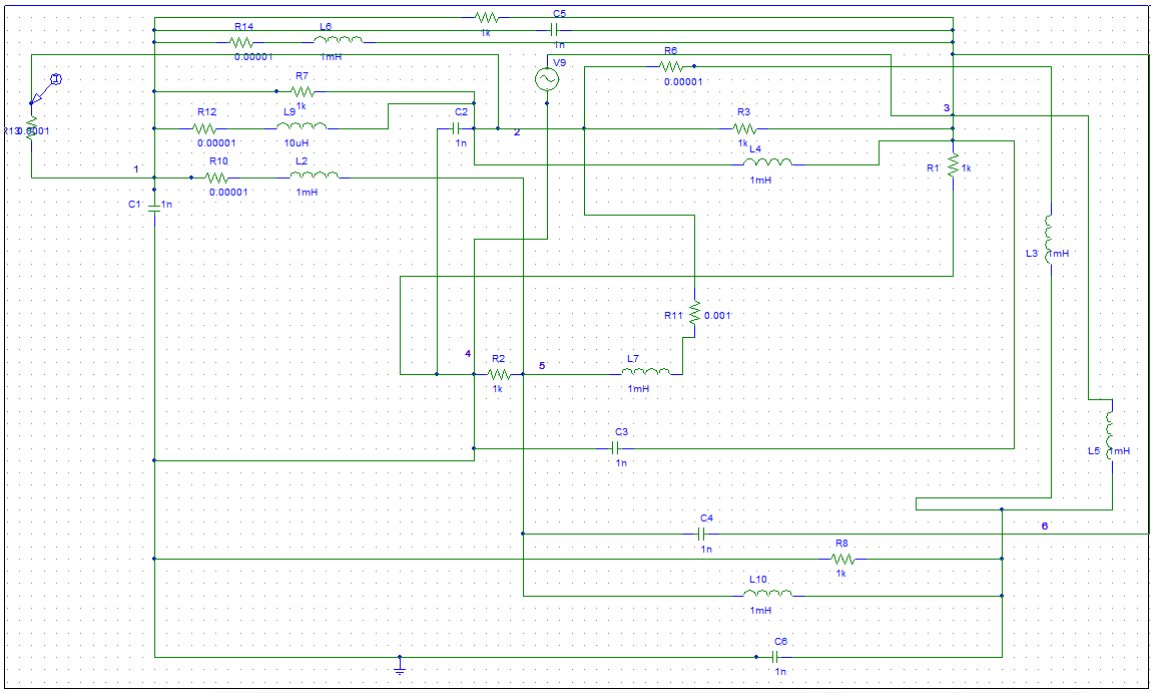

20-element circuit with drive voltage across the pair (3,4) and response current across the pair (1, 2). Compared to Fig. E.3, the drive and response terminals have been interchanged.

Reciprocity was further confirmed by changing the drive voltage to drive current, and the current response to the voltage response. That is, the drive current was applied across a pair of arbitrary terminals, while the response voltage across another arbitrary pair of terminals was measured. To show reciprocity, drive and response terminals were interchanged. The results confirmed that reciprocity also holds in this case. Two other cases (voltage being both the drive and response, and current being both the drive and response) were also tested and reciprocity was observed not to hold in these cases. The results are summarized in Table 6.

Table 6. Validity of reciprocity in electrical networks for different combinations of drive and response quantities

drive	response	reciprocity
voltage	current	yes
current	voltage	yes
voltage	voltage	no
current	current	no

There is even an additional possible type of reciprocity that we did not realize. This type was suggested by Ph.D. student David Wolfe (NPS Physics Department), who was working on piezoelectric materials. He found a calculation of the displacement of a piezoelectric material due to an applied voltage, and naturally thought that the result would hold if the same displacement was forced and the voltage was measured. However, he found that the expected reciprocal arrangement did not conserve energy. An analogous situation in a purely electrical network is to apply a voltage across one pair of terminals and measure the current through a short across the other pair of terminals, and to compare to forcing the same current through the latter pair and measuring the voltage across the former pair. However, it is straightforward to show with a simple arbitrary 3-element “T” network that this voltage is not the same as the original voltage. Hence, reciprocity does not hold in this case. In addition, the lack of reciprocity is

exhibited by the mechanical equilibrium system of a weight suspended from a horizontally stretched string undergoing linear displacements. The weight is suspended at one location, and the displacement is measured at another location. If the same displacement is forced by a weight at the location of the original displacement, the displacement at the original location of the weight is not the same.

E. CONCLUSIONS AND FUTURE WORK

Reciprocity plays important roles in the theory of transducers, especially in piezoelectric transducers that are used in underwater acoustics. One role is that reciprocity relates the transduction coefficients which quantify a transducer. Another role is that an equivalent electric circuit must exist when a transducer is reciprocal. Equivalent electrical circuits are employed because these circuits greatly simplify the analysis of the mechanical sides of a transducers. Another role of reciprocity is that it leads to a simple relationship between the receiving sensitivity and transmitting response of a reciprocal transducer. Still another role is that reciprocity can be used to calibrate a receiving transducer.

With an old demonstration apparatus consisting of a 12 x 12 grid of 1.00 k Ω resistors, we showed that reciprocity holds when the drive is a dc voltage across a pair of terminals, and the response is the dc current through a short between a different pair of terminals. The reciprocity is shown by switching the drive to the original pair of response terminals, and switching the response to the original pair of drive terminals, and observing that approximately the same current occurs. Small deviations in the reciprocity were shown to be due to the shunt resistance of the current meter. This resistance alters the network by a small amount which upsets the reciprocity.

We also investigated randomly generated electrical networks of 1.0 kΩ resistors, 1.0 nF capacitors, and 1.0 mH inductors. The random generation was accomplished by rolling dice. The first network has 10 elements, and the second

20 elements. Both networks have 6 terminals. The number of terminals was chosen so that a pair of dice can be rolled to randomly select the drive terminals, and then rolled again to randomly select the response terminals. Simulations with PSpice software showed that reciprocity holds to one part in 105, which is the precision of the software. Reciprocity was confirmed for a voltage drive and current response, as well as a current drive and a voltage response. Other possible reciprocal variables were shown not to yield reciprocity.

Future work includes the construction and testing of the 10-element randomly generated electrical network described in section C. We then plan to publish an educational journal article on lecture demonstrations of reciprocity in electrical networks. Prof. Fabio Alves (NPS Physics Department) is a co-author. Future work involves investigations of reciprocity in approximately linear equilibrium mechanical systems (Denardo, 2015), including the horizontally stretched string that is mentioned at the end of Section D. A journal article on these mechanical systems is planned to follow the electrical network article.

III. CARTESIAN DIVER

A. INTRODUCTION

A *Cartesian diver* is any compressible object that floats in a closed flexible container of liquid, which is usually water. The object is sufficiently weakly buoyant such that it sinks to the bottom when the container is squeezed. If the container is then unsqueezed, the object rises to the top. The Cartesian diver is a well-known physics demonstration and toy. Googling the name returns tens of thousands of results. The fascination is due at least in part to an apparent "action-at-distance" in causing the diver to sink and rise. The apparatus may have been discovered by René Descartes (1596–1650), but the first written account appears to be in 1648 by Galileo's student Maggiotti, who claimed the discovery (Frazier, 2015).

There are many scholarly publications on the Cartesian diver demonstration. A search for "Cartesian diver" in the educational journals (*Physics Teacher*, *American Journal of Physics*, *European Journal of Physics*, and others) yielded a total of 27 significant articles on variations and different aspects of the demonstration. In this chapter, we concentrate on interesting and challenging issues of the Cartesian diver that, to our knowledge, have not been investigated until now. None of the 27 articles is directly relevant to our work, so we have listed them in the bibliography section.

A neutrally-buoyant Cartesian diver is unstable, as we show in a demonstration and analytical treatments. One of our main motivations is the possibility of using pressure oscillations to stabilize a neutrally-buoyant object. This behavior would be essentially the same as the well-known stabilization of an inverted pendulum by vertically oscillating the support. The effect has possible applications to the utilization of a sound wave to stabilize small neutrally-buoyant probes in the ocean.

In Section B, we describe demonstrations, including a new one that conclusively shows that a neutrally-buoyant diver is unstable. Submarines are subject to this instability. In Section C, we give three *different but equivalent* explanations of the sinking of an open-bottom Cartesian diver. This is important because one explanation is appropriate for submarines, and another for scuba divers and most fish. It is also important because students often incorrectly believe that there is only *one* correct explanation. In Sections D and E, we investigate the instability of a neutrally-buoyant diver. This surprisingly leads to a hydrostatic paradox, which we resolve by allowing a compliance of the container. In Section F, we consider the possibility of parametric stabilization of a neutrally-buoyant Cartesian diver, which can occur by externally modulating a parameter upon which the strength of the instability depends. Conclusions and future work are presented in Section G.

B. DEMONSTRATIONS

One of the simplest realizations of a Cartesian diver is an open small inverted test tube partially filled with air in a common 2-liter flexible soda bottle of water (Figure 10a). The container should be completely full of water, and the test tube should be roughly half-filled with water. We wrap a piece of colored tape around the open bottom of the test tube so that it can be clearly visible in a large classroom. The container must be securely capped. When the container is sufficiently squeezed, the test tube sinks to the bottom (Figure 10b). When the container is then unsqueezed, the test tube rises to the top. We explain the behavior in the next section (Section C).

Figure 10. Cartesian diver apparatus and effects of squeezing/ unsqueezing

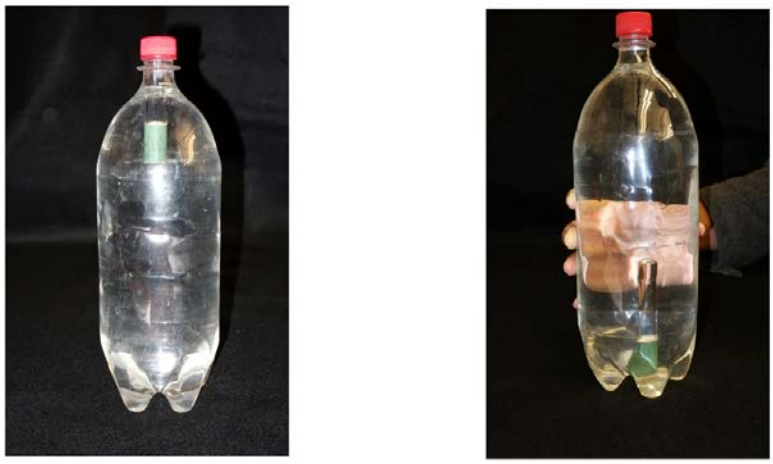

Fig. 10a. Simple version of a Cartesian diver apparatus. An inverted test tube partially filled with air floats in a closed flexible 2-liter container of water. Fig. 10b. Effect of squeezing the container. The test tube sinks to the bottom. When unsqueezed, the test tube rises to the top.

In the second demonstration, the demonstrator slowly squeezes the container by hand to achieve neutral buoyancy (buoyant force equaling the gravitational force) for the test tube roughly halfway down the container. The audience and even the demonstrator can have the false impression that this equilibrium is stable. However, as explained in Section D, the equilibrium is *unstable*. The apparent stability is due to the demonstrator continually consciously or subconsciously adjusting the pressure a slight amount to prevent the instability. To convincingly show that the equilibrium is unstable, we use a large hose clamp and a nut driver to squeeze the container (Figure 11). A large C-clamp resting on a lab jack can also be used, which has the advantage of doing much less damage to the plastic container. Carefully tightening the clamp clearly shows that the equilibrium is unstable, because the clamp has to be continually tightened and loosened to maintain the equilibrium, which is clearly visible to a large audience.

Figure 11. Effect on Neutrally-buoyant Cartesian Diver

Fig. 11a. A neutrally-buoyant Cartesian diver in a container squeezed by hand. The motion is unstable, although this is a subtle effect when squeezing by hand. Without feedback of the motion of the diver, and consequent slight increases and decreases in the squeezing, the diver will permanently rise to the top or sink to the bottom. Fig. 11b. Use of a large hose clamp to convincingly show that the equilibrium of a neutrally-buoyant Cartesian diver is unstable. The clamp has to be continually tightened and loosened to prevent the diver from permanently rising or falling.

C. EXPLANATIONS OF SINKING

The open-bottom test tube has an important advantage over Cartesian divers that are sealed. In the latter case, the body (diver) has constant mass and variable volume depending upon the amount that the container is squeezed. In the open-bottom test tube case, there are *three* different natural definitions of the body (Table 7). Clearly, the behavior must be *independent* of our choice of the body. However, a common misconception among students is that there is only *one* correct definition of the body. The open-ended Cartesian diver is thus educationally useful as an example of how our conception of a body can only be a convenience and may not be unique.

Table 7. Different possible definitions of the body in a Cartesian diver

case	body	constant quantity	application
i	glass and air	mass	scuba divers and most fish
ii	glass, air, and water inside tube	volume	submarines
iii	only glass	mass and volume	?

Different possible definitions of the body in a Cartesian diver apparatus that employs an open inverted glass test tube. Applications are listed in the column on the right. We are not aware of any applications for the third case.

We first consider case (i) in Table 7. As the bottle is squeezed, the air compresses; to a very good approximation the water is incompressible and the glass is rigid. The volume of the body decreases while its mass remains constant, so the average density of the body *increases*. Archimedes' law is that the buoyant force is the weight of the displaced fluid. Hence, when the average density of the body exceeds the density of water, the buoyant force is insufficient to prevent the body from sinking. This effect is utilized by scuba divers by pumping air out of a *buoyancy compensator*, which is a flexible vest that contracts or expands when air is pumped out of or into it. The effect is also utilized by most fish by squeezing their air bladders. In both cases, the mass remains constant but the volume decreases, which causes the sinking.

Neglecting the mass of the air in our Cartesian diver, note that the sinking is only possible if the density of the material is greater than the density of the liquid, which is true in our case because the density of glass is greater than the density of water. Once the test tube begins to sink, the air compresses even more due to the pressure gradient in the water. Hence, the test tube sinks to the bottom with an increasing speed. This may appear to be obvious. However, a

hydrostatic paradox occurs for a rigid container and incompressible liquid. This issue will be discussed in detail in section E.

To quantify the sinking, we assume that the water is incompressible and the glass is rigid. We also consider the simplified model of a test tube with a square rather than rounded bottom. The parameters are shown in Figure 12, where h is the height of the air column and A is the cross-sectional area of the air column (*inside* dimensions of the glass). We let m_a be the mass of the air, m_g the mass of the glass, and V_g the volume of the glass of the test tube. The latter two quantities are related by $m_g = \rho_g V_g$, where ρ_g is the density of the glass.

Figure 12. Parameters of a Cartesian diver system

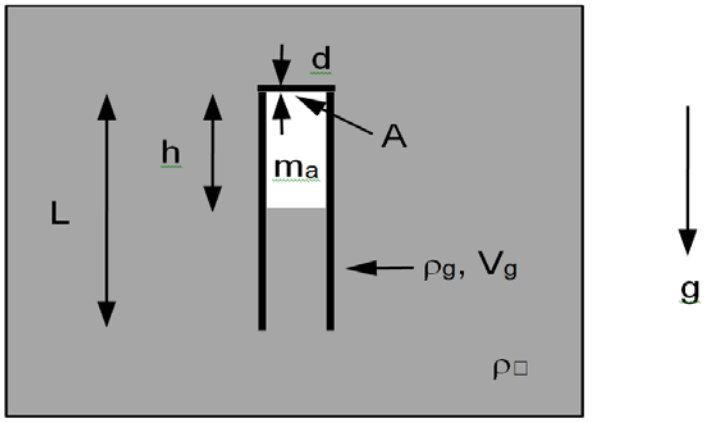

As the volume of the container is reduced, the volume of air decreases, and the body sinks when the buoyant force becomes less than the gravitational force.

The average density of the body is its total constant mass divided by its total variable volume:

$$\rho_{ave} = \frac{m_g + m_a}{V_g + Ah} . \qquad \text{(C.1)}$$

The condition for sinking is $\rho_{ave} > \rho_w$, which is readily shown to yield

$$h < \frac{1}{A}\left[m_g\left(\frac{1}{\rho_w} - \frac{1}{\rho_g}\right) + \frac{m_a}{\rho_w}\right]. \qquad \text{(C.2)}$$

If the mass of the air is negligible compared to the mass of the glass, which is typically the case, the condition (C.2) on the height of the air column for sinking reduces to

$$h < \frac{m_g}{A}\left(\frac{1}{\rho_w} - \frac{1}{\rho_g}\right), \qquad \text{(C.3)}$$

which agrees with our previous qualitative conclusion that the diver can only sink if the density of the material is greater than the density of the liquid.

The explanation of case (ii) in Table 7 is similar to the explanation of case (i), except that now the volume rather than the mass is constant. The mass increases as the bottle is squeezed, rather than the volume decreasing. Hence, the average density again increases, which eventually causes the body to sink according to Archimedes' law. This is accomplished in a submarine by pumping water into the ballast tanks. The volume of the submarine remains the same, but the mass increases, which causes the sinking.

Quantitatively, the average density of the body is the variable mass divided by the constant volume, in contrast to Eq. (C.1):

$$\rho_{ave} = \frac{m_g + m_a + \rho_w A(L-h)}{V_g + AL}. \qquad \text{(C.4)}$$

The sinking condition $\rho_{ave} > \rho_w$ can then easily be shown to correctly be identical to Eq. (C.2). Note that the L terms in Eq. (C.4) cancel when this expression is substituted in to the sinking condition $\rho_{ave} > \rho_w$.

Archimedes' law directly and readily solves cases (i) and (ii) in Table 7, but *not* case (iii), where the fluid now has two components. The condition (C.2) for sinking is consequently much more challenging to verify. The buoyant force

now has two contributions: one due to the net vertical pressure on the horizontal cross sectional area A of the upper end of the tube, which is the difference in pressure just below and above the end, and the other due to buoyant force of the water on the sides of the tube. (Refer to Figure 12.) Compared to the pressure variation with depth in the water, the pressure variation in the air is small over the height h of the air column, so the pressure just below the top of the tube will be approximately the *same* as the pressure at the bottom of the air column. The difference in pressure is thus proportional to h. The buoyant force on the vertical wall is constant. As the bottle is squeezed and h decreases, the buoyant force decreases until the net upward air pressure is no longer sufficient to prevent the tube from sinking.

To precisely determine the pressure differential on the upper end of the tube, note that the pressure differential between the top of the end and the water-air surface inside the test tube is $\rho_w g(\mathrm{h}+\mathrm{d})$, where d is the thickness of the end. The force differential between the air-water surface and the bottom of the end is the weight $m_a g$ of the column of air. The buoyant force due to the pressure differential on the area A is then

$$B_1 = \rho_w g\left(h + d\right)A - m_a g = \rho_w g\left(hA + V_{g1}\right) - m_a g, \qquad \text{(C.5)}$$

where V_{g1} = Ad is the volume of the end of the test tube. The constant buoyant force on the vertical wall can be determined from Archimedes' law as the weight of the displaced water, which is $B_2 = \rho_w g V_{g2}$, where V_{g2} is the volume of the vertical wall of the glass test tube.

Sinking occurs when the total buoyant force is less than the weight of the glass: $B = B_1 + B_2 < \rho_g V_g g$. Substituting the above expressions for B_1 and B_2, recognizing that the total volume of the glass is $V_g = V_{g1} + V_{g2}$, using $m_g = \rho_g V_g$, and simplifying, correctly yields Eq. (C.2).

We have seen that case (i) in Table 7 leads to the simplest quantitative description of the behavior of a Cartesian diver. We henceforth choose the body to be case (i).

D. OPEN-CONTAINER INSTABILITY

As shown in the second demonstration in Section B, the equilibrium of a neutrally-buoyant body is *unstable*. To understand this effect, we first consider an *open* system, where the free surface of the water is exposed to air of constant pressure p_0 (Figure 13a). If it is assumed that the water is incompressible and the glass is rigid, the condition for neutral buoyancy is given by Eq. (C.2) with an equality. The air column height for which equilibrium (neutral buoyancy) occurs is then

$$h_{eq} = \frac{1}{A}\left[m_g\left(\frac{1}{\rho_w} - \frac{1}{\rho_g}\right) + \frac{m_a}{\rho_w}\right]. \qquad \text{(D.1)}$$

We can interpret the condition (D.1) as follows. For a given test tube, and for a given mass of air m_a such that $h \geq h_{eq}$ when the top of the test tube is at the air-water surface of the container, equilibrium will occur at the depth such that the column of air has height h_{eq}.

Figure 13. Neutrally-buoyant Cartesian Diver in an Open Container

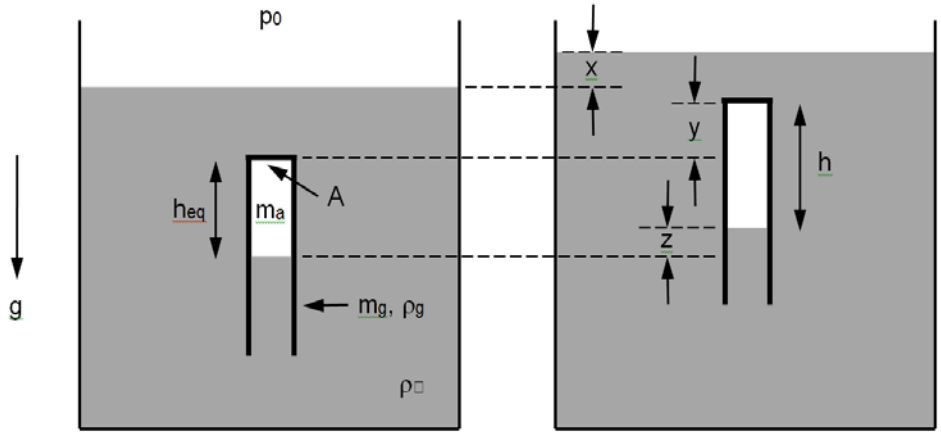

Fig. 13a. Neutrally-buoyant Cartesian diver in an open container. The constant external air pressure is p_0. Fig. 13b. Definitions of various displacements from equilibrium (neutral buoyancy).

Imagine a vertical displacement of the body from equilibrium. In general, the change in pressure will cause a change in the volume of the air in the body, which in turn will cause a change in height of the free surface of the water. However, for the case in which the container is much larger than the body, the change in height of the free surface of the water will be negligible. The pressure distribution in the water will thus be *independent* of the location of the body. For an upward displacement of the body, the pressure decreases, so the air must expand. The buoyant force then increases, so the body will continue to rise. Similarly, for a downward displacement, the buoyant force decreases, so the body will continue to fall. There is thus an *anti-restoring* force, which is responsible for the instability.

Submarines or any other actual bodies are not perfectly rigid, so they are subject to the instability. However, due to the low compliance, the effect is weak compared to the Cartesian diver. However, the instability can still be a problem, especially if the submarine is not in horizontal motion. In such motion, the bow planes can be adjusted to counter the instability.

We now quantify the instability for an open container that is much larger than the body. We will later consider the general case. We continue to assume that the water is incompressible and the glass is rigid. Because the body has constant mass, the gravitational force is constant and will thus not play a role in the anti-restoring force for deviations from equilibrium; this force is due completely to the change in the buoyancy force. In the laboratory frame of reference, we let y denote the vertical displacement of the test tube from equilibrium, and z denote the vertical displacement of air-water surface in the test tube from equilibrium (Figure 4b). Neutral buoyancy corresponds to y = 0 and z = 0. We choose y and z to be positive upward. The change in height of the air column is $\Delta h = h - h_{eq} = y - z$. By Archimedes' law, the change in the buoyancy force is then

$$\Delta B = \rho_w g A \Delta h . \qquad \text{(D.2)}$$

We seek ΔB as a function of the displacement y. The boundary condition on the air-water surface in the test tube is that the pressure is *continuous*. The pressure deviation from neutral buoyancy on the water side of the air-water surface in the test tube is

$$\Delta p = p - p_{eq} = -\rho_w g z = \rho_w g(\Delta h - y) . \qquad \text{(D.3)}$$

We need to determine the pressure deviation on the air side, and then set the two pressure deviations equal in order to satisfy the boundary condition. The force due to the mass of air m_a in the gravitational field is constant and thus combines with other forces to yield net zero force in equilibrium. We then need to calculate the deviation in *thermodynamic* pressure. We assume that the process is adiabatic. The pressure and volume of the air in the test tube thus obey pV^γ = constant = $p_{eq} V^\gamma{}_{eq}$, where γ is the ratio of the specific heats of air. The isothermal result can be simply found by setting γ = 1 at the end of the

calculation. The deviation in the thermodynamic pressure (excess pressure) of the air in the test tube is

$$\Delta p = p - p_{eq} = p_{eq}\left[\left(\frac{V_{eq}}{V}\right)^{\gamma} - 1\right] = \frac{m_a R T_{eq}}{M_a A h_{eq}}\left[\left(\frac{h_{eq}}{h_{eq} + \Delta h}\right)^{\gamma} - 1\right] \quad \text{(D.4)}$$

where $V_{eq} = Ah_{eq}$ and $V = Ah = A(h_{eq} + \Delta h)$. In addition, we have used the ideal gas law to determine the equilibrium pressure p_{eq}, where R is the universal gas constant, T_{eq} is the equilibrium absolute temperature, and M_a is the molar mass of air. Equating the expressions (D.3) and (D.4) for the deviation in pressure yields an equation that *cannot* be analytically solved for Δh. We thus consider small deviations from equilibrium. To first order in $\Delta h/h_{eq}$, Eq. (D.4) yields

$$\Delta p = -\frac{m_a c^2}{A h_{eq}^2}\Delta h\,, \quad \text{(D.5)}$$

where we have used the square speed of sound $c^2 = \gamma RT_{eq}/M_a$ in air. Setting the pressure deviations (D.3) and (D.5) equal, solving for Δh, and substituting the resultant expression into the deviation of buoyancy (D.2) yields

$$\Delta B = \frac{\rho_w g A}{1 + m_a c^2 / \rho_w g A h_{eq}^2}\, y\,, \quad \text{(D.6)}$$

which is valid for small deviations from equilibrium. Note that $\Delta B > 0$ for $y > 0$ and that $\Delta B < 0$ for $y < 0$, so the force is indeed anti-restoring, as we previously concluded qualitatively. We can check the result (D.6) in two special mathematical (although unphysical) cases: $\gamma = 0$ and $\gamma = \infty$. From the adiabatic condition pV^{γ} = constant, the case $\gamma = 0$ corresponds to constant air pressure, which can only occur if the bottom of the air plug remains at the same location in the container. The change in volume of the air is then simply Ay, so the change in buoyancy is $\Delta B = \rho_w gAy$. The expression (D.6) precisely reduces to this

result because c = 0 for $\gamma = 0$. Next, the adiabatic condition for $\gamma = \infty$ corresponds to constant volume of the air plug, because nonconstant volume would imply infinite pressure. In this case, the change in buoyancy must be zero, which is precisely to what the expression (D.6) reduces, because c = 0 for $\gamma = \infty$.

One may wonder why we did not have to deal with the thermodynamics in Sec. C, whereas we had to deal with it here. The reason is that we did not have to calculate the amount of squeezing required to sink the test tube; we only calculated the critical value of the height h of air in the test tube.

In the above calculation, we assumed a large (strictly infinite) container. What effect if any does a *finite* container have on the instability? An upward displacement of the test tube should still cause the volume to increase due to a reduction of pressure at the water-air interface in the test tube. The level of the water in the container must then rise, which will cause the pressure at the interface to increase. Hence, the instability should still occur, but be *weaker* compared to the case of a relatively large container.

Quantitatively, let A_c be the cross-sectional area of the container. The expression (D.6) is the approximate change in buoyancy corresponding to $A/A_c << 1$, for which the change in surface height in the container is negligible. For an arbitrary value of $A_c > A$, we let x equal the vertical displacement of the surface for a vertical displacement y of the test tube. Conservation of the total mass of the incompressible liquid dictates that $A_c x = A \Delta h$. The change in buoyancy (D.2) and the thermodynamic pressure of the air (D.5) still hold. However, in the change in pressure (D.3) at air-water surface in the test tube, we now must replace z with z – x:

$$\Delta p = -\rho_w g(z - x) = \rho_w g\left[\left(1 + \frac{A}{A_c}\right)\Delta h - y\right]. \qquad \text{(D.7)}$$

Carrying the additional A/A_c term through the calculation leading to Eq. (D.6) yields

$$\Delta B = \frac{\rho_w g A}{1 + m_a c^2 / \rho_w g A h_{eq}^2 + A/A_c} y \ . \qquad \text{(D.8)}$$

Note that this result correctly reduces to the special case (D.6) when $A/A_c = 0$ (or $A_c = \infty$). In the general case, the A/A_c term explicitly shows that a finite-size container causes a reduction in strength of the instability, in accord with our previous qualitative argument.

E. CLOSED-CONTAINER INSTABILITY

We now investigate a neutrally-buoyant Cartesian diver test tube in a *closed* container. We first consider the ideal system in which the liquid is incompressible and both the glass and container are rigid. Is the equilibrium unstable? Due to the constant vertical pressure gradient in the liquid, which is necessary because the liquid is a gravitational field, the air must expand for an upward displacement and contract for a downward displacement, so the instability *should* occur. However, due to the incompressibility of the liquid and rigidity of the container, the air volume must remain the same, so the instability should *not* occur; specifically, neutral stability should occur. We thus have a hydrostatic paradox!

Note that this is not the *standard* hydrostatic paradox, which involves the fact that the pressure at the bottom of a container of liquid in a gravitational field depends only upon the height of the liquid and not the cross-sectional area. This fact leads to what appear to be contradictions. For example, a thin column of liquid connected to a wide column can support and even lift a heavy weight on a wide column. In another example, the bottoms of a straight cylinder and a truncated conical cylinder have the same cross-sectional areas and rest on separate balances. Both cylinders contain the same height of water. The pressures at the bottom must be the same, but the weights will be different. (Physics Stack Exchange, 2015).

It is natural to suspect that the paradox in our case is due to the assumption of either a perfectly rigid container or an exactly incompressible liquid. A flexible container is appropriate to consider for a Cartesian diver. In addition, a compressible liquid appears to be more difficult to calculate due to the lack of a uniform pressure gradient with depth. We thus consider a flexible container. A model system of a neutrally-buoyant Cartesian diver in a flexible container is shown in Fig. 5. The system is a simple and natural generalization of the open container system in Fig. 4. We choose the spring to be unstretched when the diver is in equilibrium. A more appropriate parameter than the spring constant k is the stress modulus $\kappa = k/A_c$.

Figure 14. Model system of a neutrally-buoyant Cartesian diver in a closed compliant (nonrigid) container

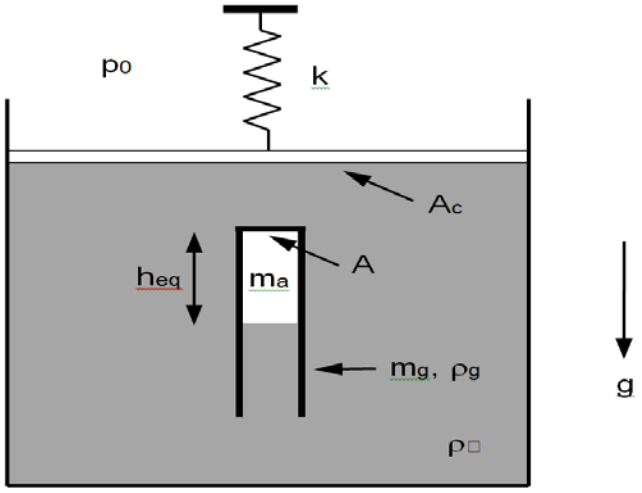

Model system of a neutrally-buoyant Cartesian diver in a closed compliant (nonrigid) container. The spring is connected to a piston that is massless and frictionless.

First, we consider a very large (strictly infinite) closed container. Because the change in the level of water in the container is negligible when the body undergoes vertical displacement, the development is identical to that for a very large open container in the previous section (Section D), where p_0 is now the

pressure exerted by the piston on the liquid. That is, the spring has no effect. Hence, the system is unstable, and is quantitatively described by the condition for neutral equilibrium (D.1) and the change in buoyancy (D.6) for small displacements of the body.

For a finite closed container in which the body is displaced upward from equilibrium, the air must expand due to the lower pressure, which causes the level of water in the container to rise. Due to the spring, however, the pressure will increase in the water, which reduces the increase in volume of the air. The change in buoyancy is thus reduced, so the instability is *weakened*.

As in the quantitative development in Section D, we let x be the displacement of the container's water level due to a small displacement of the diver. Also as in that section, conservation of the total mass of the incompressible liquid dictates that $A_c x = A\Delta h$. In addition, the change in buoyancy (D.2) and the thermodynamic pressure deviation of the air (D.5) still hold. By Pascal's law, however, to the change in pressure (D.7) at air-water surface in the test tube, we now must add the pressure due to the piston:

$$\Delta p = \frac{kx}{A_c} - \rho_w g(z - x) = \left[\frac{kA}{A_c^2} + \rho_w g\left(1 + \frac{A}{A_c}\right)\right]\Delta h - \rho_w g y . \quad \text{(E.1)}$$

Setting $k/A_c = \kappa$, and carrying the additional κ term through the calculation in Sec. D yields

$$\Delta B = \frac{\rho_w g A}{1 + m_a c^2 / \rho_w g A h_{eq}^2 + \left(1 + \kappa / \rho_w g\right) A / A_c}\, y . \quad \text{(E.2)}$$

Note that this expression correctly reduces to the open container result Eq. (D.8) for the special case $\kappa = 0$. The expression explicitly shows that the stiffness of the container causes a *reduction* in strength of the instability, which is in accord with the above qualitative argument. In the limit of a rigid container ($\kappa \to \infty$), the instability *vanishes*; $\Delta B = 0$ and the body is neutrally stable. We can now resolve

the paradox, which occurs due to the constant vertical pressure gradient in the liquid. For an upward displacement of the body from equilibrium, an overall pressure increase occurs. This increase in pressure exactly cancels the reduction in pressure due to the gradient, so the volume of air remains the same as it must.

F. PARAMETRIC STABILIZATION

In general, an oscillator can be excited if a parameter upon which the natural frequency depends is modulated. This is the well-known phenomenon of *parametric excitation* (Landau and Lifshitz, 1976; Denardo, 2012). The standard example is a pendulum in a gravitational field. If the support is vertically oscillated, the equilibrium state can become unstable, and transverse oscillations of the pendulum can occur. In the noninertial frame of reference in which the support is at rest, the acceleration due to gravity is modulated, and the frequency of oscillations depends upon this parameter.

In a sense, the phenomenon is *reciprocal*: An unstable equilibrium state of an oscillator can be become stable if a parameter upon which the strength of the instability depends is modulated (Landau and Lifshitz, 1976; Denardo, 2012). We refer to this phenomenon as *parametric stabilization*. The standard example is again a pendulum in a gravitational field, only now the inverted equilibrium state is considered. This state is clearly unstable. However, when the support is vertically oscillated for a specific range of frequencies and amplitudes, the motion can be stabilized.

It is natural to wonder if the unstable equilibrium of a Cartesian diver (Secs. D and E) can be stabilized by externally modulating the pressure, the acceleration due to gravity, or some other parameter. The first case may be achieved by driving a piston or by squeezing a flexible container. Another possibility, which could be practical in the ocean, is a sound wave whose wavelength is substantially greater than the size of the driver. The case of

modulating the acceleration due to gravity can be achieved by vertically oscillating the container.

Quantitatively, we consider the general model in Figure 5. The change in buoyancy for a small vertical displacement y of the diver from equilibrium is given by Eq. (E.2). The strength of the instability depends upon many parameters. Some of these parameters, namely, ρ_w, m_a, c, A, and A_c, as well as h_{eq} in Eq. (D.1), would be very difficult or impossible to modulate. The acceleration due to gravity g and the stress modulus κ can be modulated. The first can be done by vertically shaking the container, as stated above. In regard to the second, it should be noted that a mechanical compliance (inverse of the stiffness) is analogous to an electrical capacitance in equivalent electrical circuits, and it is easy to image ways of modulating a capacitance. However, it appears to be difficult to modulate the stiffness here.

It is perhaps surprising that the external pressure p_0 does *not* alter the strength of the instability. As described above, a pressure modulation can be readily achieved, but what effect does it have on the motion of a diver? The volume of the air will change, which will change the buoyancy. For a small displacement y from equilibrium, and for a small pressure modulation $\Delta p_0 = P\cos(\omega t)$, the total change in buoyancy will just be the sum of the two effects, which has the form

$$\Delta B = \alpha' y - \beta' P \cos(\omega t) , \qquad \text{(F.1)}$$

where α' and β' are positive constants, and where P is the amplitude of the pressure modulation and ω is the frequency. By Archimedes' law, the equation of motion will then have the form

$$\ddot{y} + \mu\dot{y} - \alpha y = -\beta P \cos(\omega t) , \qquad \text{(F.2)}$$

where α, β, and μ are positive constants, and where μ is a damping parameter. The linear equation of motion (F.2) represents a unstable system that

is directly acted upon by an oscillatory drive. The homogeneous solution has an exponential instability and the particular solution sinusoidally oscillates. The motion thus exhibits oscillations but is unstable. We conclude that a modulation of the external pressure *cannot* stabilize the system, at least for the relatively small displacements and drive amplitudes that we have assumed in order to make analytical progress.

G. CONCLUSIONS AND FUTURE WORK

The Cartesian diver is an old and popular physics demonstration and toy. We have presented a simple demonstration of the sinking and rising with a closed flexible 2-liter soda bottle filled with water and containing an inverted glass test tube partially filled with air. Squeezing the bottle by hand causes the diver to sink; unsqueezing causes the diver to rise. There is a substantial amount of literature on the Cartesian diver. We have investigated aspects that we have not found in the literature.

A constant squeezing by a specific amount causes the diver to be suspended in equilibrium below the top. This equilibrium state is unstable, although this may not be apparent to an audience or even to the person who squeezes the container. Use of a large hose clamp and a nut driver clearly shows that the instability exists, because the person must continually tighten and loosen the clamp to maintain the equilibrium. A large C-clamp can alternatively be used.

The standard explanation of the sinking of a Cartesian diver involves defining the diver to be the glass and the air. The diver therefore has constant mass. Squeezing the container compresses the air and thus reduces the volume of the diver. Once the average density increases beyond the density of water, the diver will sink. However, there are two other possible definitions of the diver: the glass plus the air and water inside the test tube, and just the glass itself. We have qualitatively and quantitatively shown that the identical result for sinking

occurs for these alternative definitions of the body. The alternative approaches are important for several reasons. First, one way that submarines sink or rise is by pumping water into or out of the ballast tanks, which corresponds to the case of constant volume and variable mass. In contrast, the rising and sinking of scuba divers and most fish correspond to the case of constant mass and variable volume. Second, students often think that the diver can *only* be defined as having constant mass, which is incorrect. Third, our results show that the standard choice of constant mass turns out to be the easiest one to handle for the complicated analytical stability calculations that we have presented. However, we did not know this fact until we established it.

The stability calculations involve the determination of the change in buoyancy of a neutrally-buoyant Cartesian diver in both an open and closed container. The change in buoyancy is the force on the diver when it is displaced from equilibrium, and we qualitatively and quantitatively showed that this force is anti-restoring for small displacements, which is why the diver is unstable. Our calculations are for a model system that unites open and closed containers, and incorporates a nonzero compliance of the container. This compliance is necessary in order to avoid a hydrostatic paradox which is distinct from the standard paradox that is in the literature.

We used our quantitative results for the change in buoyancy to show that it is theoretically impossible to parametrically stabilize a neutrally-buoyant Cartesian diver by external oscillations of the pressure. Such pressure oscillations would occur due to a sound wave, and the stabilization by this method could have useful practical applications in the ocean. However, we did show that modulation of the gravitational acceleration, which can be achieved by vertically shaking a container, can theoretically yield parametric stabilization of a diver. This fact may have applications in processing or observation of reactions of chemical and biological substances that must not come in contact with the walls of the container.

Future work based on our results can be done in several areas:

A student survey on the three possible explanations of the sinking of the Cartesian diver should be done. The goal of the survey would not only be to quantitatively probe the students knowledge of fluid mechanics but also whether or not they believe there can be more than a single correct explanation for a physical phenomenon.

We resolved the hydrostatic paradox in our case by considering a compliant container. Alternatively, it should be possible to resolve the paradox by considering a compressible liquid. This is a challenging problem because the density of the liquid will vary with depth. The problem is important for a complete a understanding of the Cartesian diver, and may yield one or more surprises.

A demonstration and quantitative experiment can be done on the predicted parametric stabilization of a neutrally-buoyant Cartesian diver by vertical shaking. As stated above, this effect has applications to containerless processing and observation of some chemical and biological reactions. In addition, it would be educationally important as a novel demonstration of parametric stabilization in addition to the standard demonstration of an inverted pendulum. It may be useful to first do computer simulations before attempting an experiment, in order to verify the stabilization and to ascertain whether it can be practically achieved. Finally, even though our theory predicts that parametric stabilization by external pressure modulation is impossible, the effect still may be possible for reason or reasons that are currently unknown. Due to the importance of applications using sound waves in the ocean, the possibility should be probed with computer simulations and experiments.

THIS PAGE INTENTIONALLY LEFT BLANK

IV. NECKLESS HELMHOLTZ RESONATORS

A. INTRODUCTION

A relatively long wavelength acoustic resonance can occur in a cavity with an open neck. This resonance is commonly excited by using the mouth to blow air across the open neck, and such a resonator is called a *Helmholtz resonator*. Various glass bottles are familiar examples. Other examples include large drinking water containers (even 5-gallon containers!), Christmas ornament bulbs with the stems removed, and a musical instrument called the *ocarina*. An example that is particularly annoying for parents is when children clasped their hands with side-by-side thumbs to form a cavity with a neck. Because the wavelength corresponding to a Helmholtz resonance is typically much larger than the size of the resonator, the system can be considered effectively as the "lumped" system of a mass on a spring. The rigid motion of air in the neck supplies the inertia, and the uniform compressions and expansions of air in the cavity supply the stiffness. A simple formula for the frequency can then easily be derived (Kinsler et al., 2000). However, this formula ignores corrections due to the flow at the ends of neck.

A Helmholtz resonator that is excited by a steady flow across the open neck is an example of a *maintained* or *self-excited* oscillator. These oscillators are often very difficult to fully and correctly explain. The Helmholtz case falls into the musical category of flutes, and these maintained oscillators are very difficult to explain. The standard simplistic explanation, which is given by Benade (1990), is that the mode causes the external flow to divert inward when the flow velocity of the mode is inward, and outward when the flow velocity is outward, so a net positive work is done by the external flow on the mode. However, this explanation not complete, and may not even yield a phase that causes a net positive energy to be fed into the oscillations. The explanation is also incomplete because it is known that vortex shedding plays a fundamental role in the

excitation. We are not aware of any proper qualitative explanation of the maintained excitation of flutes. A quantitative and lengthy detailed explanation is given by Fletcher and Rossing in their book on the physics of musical instruments (1998).

In the 1800s, Helmholtz and others used Helmholtz resonators to determine the frequency of a pure tone or the spectrum of a multifrequency tone (Helmholtz, 1954). A small nipple was located on the other side of the neck. An investigator would either insert the nipple directly into an ear or use a small tube to connect the nipple to an ear. This was a very slow way and only roughly approximate way of achieving what is today easily and accurately found with a fast-Fourier transform analyzer.

Helmholtz resonances are utilized in stringed musical instruments in order to increase the amplitudes of low frequencies. Examples are the f-holes in violins and the circular hole in the top of acoustic guitars. Rossing (2007) states that "The use of a [Helmholtz] resonance air cavity to boost the low-frequency response has been a common feature of almost every stringed instrument from ancient times." Another application of Helmholtz resonances in musical instruments is the mouthpieces of brass instruments. A Helmholtz resonance of the mouthpiece causes a "popping" frequency which drives the ultimate sound from the instruments (Rossing, 2007).

There are many modern applications of Helmholtz resonators. They are often used to dampen sound in ducts, including automobile mufflers. Helmholtz resonators are also incorporated into the walls of buildings in order to absorb unwanted sound (Rossing, 2007). Double Helmholtz resonators, which consist of two cavities connected by a neck, have been employed to accurately determine some transport properties of gases (Gillis and Moldover, 2014). In addition, Helmholtz resonators have been used for source amplification in systems other than musical instruments. A very prevalent example is a ported loudspeaker enclosure which enhances low frequencies due to a Helmholtz resonance

(Rossing and Fletcher, 2004). This construction is called *bass reflex*. Another example of a Helmholtz resonator is one that has been developed for use as a low-frequency source of sound in water (Wilson, 1989). Other applications can be found in Wikipedia (2015a).

Synthetic jets (Glezer and Amitay, 2002) is a new field of research that involves Helmholtz resonators. These systems are small internally driven Helmholtz resonators that create a steady outward jetting flow. One possible application is the control of the separation of a boundary layer from a wing, which could substantially reduce drag.

Helmholtz resonators have been proposed as sources of low-frequency underwater sound (Wilson, 1989). The can also be unintentional sound sources on the surfaces of submarines (Arunajatesan and Sinha, 2005). Not surprising due to modern society's high level of energy consumption, Helmholtz resonators have been proposed for energy harvesting (Atra and Salleh, 2013). Automobiles with a partially or fully open side window can exhibit very annoying low-frequency Helmholtz oscillations on freeways and other roads (An et al., 2004).

Helmholtz resonances can occur in the surface level of water in a bay with a narrow inlet (Blanchfield et al., 2008) or harbor with a narrow inlet (Rabinovich, 2009). The resonances can be driven by semidiurnal (twice-a-day) or diurnal (once-a-day) tides, or by tsunamis. The large semidiurnal tidal elevation range of 14.5 m in the Bay of Fundi in Canada corresponds to a *quarter-wavelength* resonance rather than a Helmholtz resonance (Wikipedia, 2015b).

A Helmholtz resonator need *not* have a physical neck. The geometrical neck length could be *zero*, which was recognized by Helmholtz himself (Helmholtz, 1954). An *effective* neck exists due to the constriction of the flow, which is quantified by the end correction. Examples of these Helmholtz resonators are the above cases of violins, guitars, automobiles with lowered side windows, and some bays and harbors. Our objective in this chapter is to investigate neckless Helmholtz resonators. One of our motivations is to obtain a

lecture demonstration that dramatically shows the existence of end corrections. Another motivation is due to the fact that the theoretical end correction is based on the assumption that the flow near an opening acts as a rigid piston. This is reasonable when an appreciable physical neck exists, because a column of air exists. When there is no neck, however, the assumption may not be valid. The flow could diverge more quickly, which would lower the inertia and thus increase the frequency.

In Section B, we describe our neckless spherical Helmholtz demonstration. In Sections C and D, we compare theoretical and experimental values of the resonance frequency of the spherical demonstration Helmholtz resonator. Some of this work was done with a previous NPS thesis student (Emerson, 2015). We performed additional experiments and also improved the precision. In Sections E and F, we compare theoretical and experimental values of the resonance frequency for a precision cylindrical Helmholtz resonator. Conclusions and future work are presented in Section G.

B. LECTURE DEMONSTRATION

Our lecture demonstration apparatus of a neckless Helmholtz resonator is a thin plastic sphere with a hole in it (Figure 15). The approximate dimensions of the resonator are: outer diameter 6.0 in, thickness 0.070 in, and hole diameter 1.0 in. Blowing across the hole can cause the Helmholtz mode to be excited and clearly heard, although the tone is somewhat “rough” rather than pure. To detect the sound, we use a microphone connected to an FFT signal analyzer, which yields frequencies in the approximate range

$$f_{demo} = 195\,\text{Hz} - 215\,\text{Hz} = (205 \pm 10)\,\text{Hz}$$

where the low and high frequencies correspond to the minimum and maximum flow velocities, respectively, for excitation of the sound by mouth.

Figure 15. Spherical demonstration Helmholtz resonator, and approximate dimensions

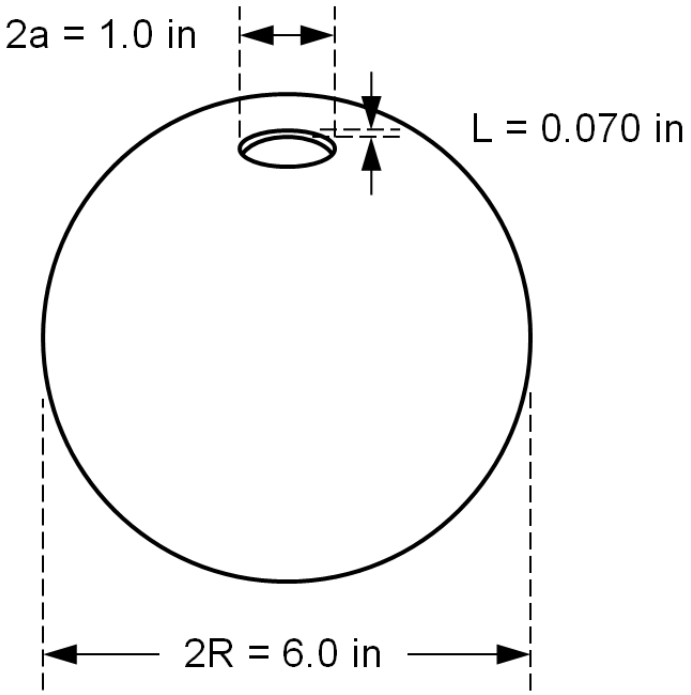

Spherical demonstration Helmholtz resonator. This Helmholtz resonator is "neckless;" the length L of the neck is small compared to the diameter 2a of the opening.

In general, the theoretical frequency of the Helmholtz resonator in Figure 16 is (Kinsler et al., 2000)

$$f = \frac{c}{2\pi}\sqrt{\frac{S}{L_{eff}V}}\ , \qquad \text{(B.1)}$$

where c is the speed of sound, S is the area of the opening, V is the volume of the cavity, and L_{eff} is the effective length of the neck. For an ideal baffle (infinite planar flange) at both ends of the neck, the effective length for a circular opening is

$$L_{eff} = L + 1.70a\ , \qquad \text{(B.2)}$$

where L is the geometrical length of the neck and a is the radius of the opening. The second term represents the *end correction*. For a Helmholtz resonator, the end correction is derived from the theory of a pipe with wavelength $\lambda >> a$, where it is assumed that the fluid at the opening acts as a piston.

Figure 16. Dimensions for determining the theoretical resonance frequency of a flanged Helmholtz resonator with a circular opening

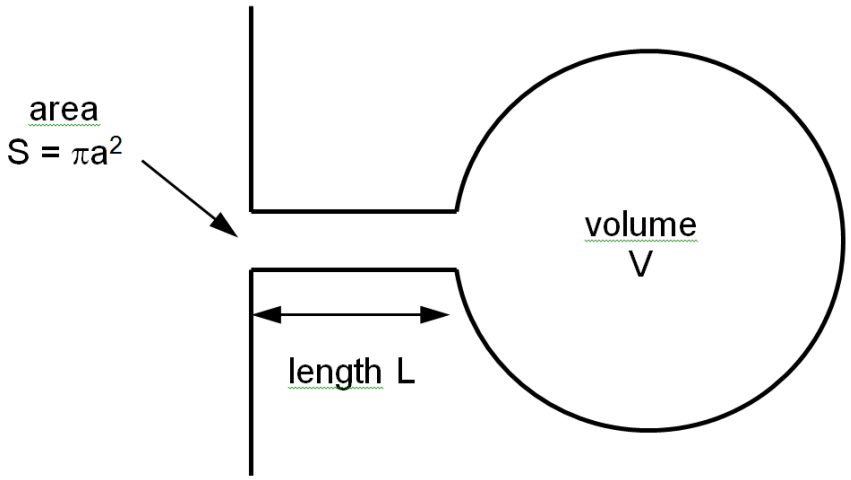

In our case, the geometric length of the neck is L = 0.070 in, and the radius of the opening is a = 0.50 in. If we ignore the end correction, the theoretical frequency for the speed of sound corresponding to 20°C is, from Eq. (B.1),

$$f_0 = \frac{(343\ \text{m/s})(39.37\ \text{in/m})}{2\pi}\sqrt{\frac{\pi(0.50\ \text{in})^2}{(0.070\ \text{in})\frac{4}{3}\pi\left(\frac{6.0\ \text{in}}{2} - 0.070\ \text{in}\right)^3}} = 701\,\text{Hz}$$

This value is a more than a factor of 3 greater than the experimental values, which dramatically shows the importance of the end correction in this case. This is the primary motivation behind the demonstration.

The effective length of the neck (B.2) for our spherical Helmholtz resonator is

$$L_{eff} = 0.070\,\text{in} + 1.70 \times 0.50\,\text{in} = 0.92\,\text{in}. \qquad \text{(B.3)}$$

The corresponding theoretical value of the frequency (B.1) is then

$$f = \sqrt{\frac{L}{L_{eff}}}\, f_0 = \sqrt{\frac{0.070}{0.92}}\, 701 = 193\,\text{Hz}.$$

The deviation between this theoretical value and the average experimental value of 205 Hz is 6%. The experimental value is greater than the theoretical value, which is qualitatively consistent with a possible breakdown of the theoretical assumption that the flow at the opening acts as a piston. The actual flow is expected to have a greater divergence, which would decrease the effective inertia and thus increase the frequency.

The theoretical value of 193 Hz is suspiciously near the 195 Hz low end of the experimental range. This prompted us to perform a controlled blower experiment to probe the minimum flow velocity for excitation of the resonator. We connected a Variac transformer to the 120 V blower to control the voltage. Experimentation led to the use of a funnel taped to the end of blower hose. The small end of the funnel has diameter 5/16 in, which produces a narrow jet of air. The minimum flow for excitation corresponds to 11.5 V, which produced a low-amplitude pure tone response of the resonator, in contrast to the somewhat rough tone produced by mouth. Surprisingly, the measured frequency was not near 195 Hz but, rather, 210 Hz. This result suggests two conclusions. First, the excitation of a Helmholtz resonator by a steady flow of air is a complicated process. Specifically, the frequency does not depend solely upon the speed of the flow. Second, the experimental and theoretical frequencies may not agree within experimental error. In Sections C and D, we develop a more careful comparison of experiment and theory, in which a loudspeaker is used for

excitation of the Helmholtz resonance, and where error analyses are done for both the experimental and theoretical values.

C. SPHERICAL SHELL THEORY

In this section, we accurately determine the theoretical prediction and uncertainty of the demonstration neckless spherical Helmholtz resonator in Section B. Accurate measurements of the dimensions, as well as the temperature at which the experiment (Section D) was done, are:

$$2R = (6.000 \pm 0.012)\,\text{in} \qquad 2a = (1.000 \pm 0.002)\,\text{in}$$

$$L = (0.069 \pm 0.001)\,\text{in} \qquad T = (25.2 \pm 0.3)\,^{\circ}\text{C}$$

Values for the uncertainties of the outer diameter 2R of the sphere and the diameter 2a of the opening were estimated by making a number of measurements and subtracting the smallest measurement of each from the largest measurement and dividing by 2. The value of the uncertainty of the temperature was determined by estimating the possible error in temperature throughout the experiment. We accurately measured the thickness L by taping a small ball bearing to the fixed side of a micrometer, measuring the distance, and then subtracting the diameter of the ball bearing. Direct measurement with the calipers yields 0.071 in, which is systematically greater than the actual value of 0.069 in part due to the curvature of the inside surface.

From the above dimensions, the area of the opening, volume, and effective neck length (B.3) are

$$S = \pi a^2 = \pi(0.500\,\text{in})^2 = 0.785\,\text{in}^2,$$

$$V = \frac{4}{3}\pi R^3 = \frac{4}{3}\pi\left(\frac{6.000}{2} - 0.069\right)^3 = 105\,\text{in}^3,$$

$$L_{\text{eff}} = 0.069\,\text{in} + 1.70 \times 0.500\,\text{in} = 0.919\,\text{in}.$$

The theoretical resonance frequency (B.1) at room temperature T_0 = 20°C, for which the speed of sound is 343.2 m/s in dry air, is then

$$f_{room} = \frac{c}{2\pi}\sqrt{\frac{S}{L_{eff}V}} = \frac{(343.2\ m/s)(39.37\ in/m)}{2\pi}\sqrt{\frac{0.785\ in^2}{(0.919\ in^2)(105\ in^3)}} = 194.0\ Hz$$

The theoretical value for the experiment is found by multiplying this value by (T/T0)1/2, where T0 = 293.15 K, and where T is the average absolute temperature during the experiment (Section D), because the frequency is proportional to the speed of sound, which is proportional to the square root of the absolute temperature. The result for the theoretical resonance frequency is then

$$f = \sqrt{\frac{T}{T_0}}\, f_{room} = \sqrt{\frac{298.35}{293.15}}\, 194.0 = 195.7\ Hz$$

.

The uncertainty of the theoretical resonance frequency is due to errors in the length measurements and to uncertainty in the speed of sound due to the uncertainty of the temperature. The estimated theoretical uncertainty is determined as follows. The resonance frequency (1) is

$$f = \frac{c}{2\pi}\sqrt{\frac{S}{L_{eff}V}} = \frac{c}{2\pi}\sqrt{\frac{\pi a^2}{(L+1.70a)\frac{4}{3}\pi R^3}}.$$

Because the length L is small compared to the radius a, the frequency is approximately

$$f = \frac{c}{2\pi}\sqrt{\frac{\pi a^2}{(1.70a)\frac{4}{3}\pi R^3}} = \frac{c}{2\pi}\sqrt{\frac{a}{(1.70)\frac{4}{3}R^3}} = \frac{c}{4\pi}\sqrt{\frac{3}{1.70}}\left(\frac{a^{1/2}}{R^{3/2}}\right).$$

Taking the differential of f due to $\delta a/a$, $\delta R/R$, and $\delta c/c = \delta T/2T$, and adding the results for a worst-case error analysis for yields

$$\frac{\delta f}{f} = \frac{\delta a}{2a} + \frac{3\delta R}{2R} + \frac{\delta T}{2T}.$$

From the above dimensions and temperature, and their uncertainties, the worst-case uncertainty of the frequency is

$$\delta f = \pm(196\ \text{Hz})\left[\frac{1}{2}\times\frac{0.002}{1.00} + \frac{3}{2}\times\frac{0.012}{6.00} + \frac{1}{2}\times\frac{0.3}{298}\right].$$

$$= \pm(196\ \text{Hz})\left[0.0010 + 0.0030 + 0.00050\right] = \pm 1\ \text{Hz}.$$

The uncertainty is ±0.5%. The final value of the theoretical frequency is then

$$f = (196 \pm 1)\ \text{Hz}.$$

A possible systematic error that could cause this frequency to be outside the calculated uncertainty is one or more protrusions in the cavity of sphere. To quantify this, and as a check on our volume calculation, we carefully used small glass beads to fill the cavity. We then poured the beads into a large graduated glass cylinder to determine the volume, which was determined to be 1705 ml with an uncertainty somewhat less than ±5 ml. The geometrically determined value (see above) is V = 105 in^3 = 1720 ml. There is nearly a 1% difference in the values, which causes a nearly 1/2% increase in the theoretical frequency. This reduces the disagreement of the experimental and theoretical resonance frequencies (refer to Section D). However, the reduction is relatively small compared to the 5% deviation between the theoretical and experimental frequencies, so the error in the volume determination is *not* responsible for the discrepancy.

D. SPHERICAL SHELL EXPERIMENT

In this section, we present accurate measurements of the resonance frequency of the demonstration neckless spherical Helmholtz resonator. We also

compare this experimental resonance frequency to the theoretical resonance frequency in Section C.

The experimental setup uses a loudspeaker driven by a function generator and power amplifier to excite the Helmholtz mode of the spherical resonator. A microphone output is filtered through a Stanford Research Systems model SR560, which also supplies a variable gain. The frequency is adjusted on the function generator until voltage reading on a multimeter is maximized. Figure 17 shows the experimental setup. The temperature during the experiment was T = (25.2 $\pm$ 0.3) ^{o}C.

Figure 17. Experimental setup for determining resonance frequency of a neckless spherical Helmholtz resonator

The experimental resonance frequency was determined to be

$$f_{exp} = (206.4 \pm 0.4)\,\text{Hz}.$$

Similar results occurred for two different methods: blowing across the top and using an FFT signal analyzer (Section B), and using the PH3451 laboratory set-up with a microphone suspended in the cavity with small wire leads passing through the neck. A more accurate method was developed for the cylindrical Helmholtz shell experiment (Section F), where a lock-in amplifier was used to reduce voltage fluctuations. The value of the resonance frequency of the spherical resonator at the same temperature was determined with the lock-in amplifier to be (206.3 $\pm$ 0.2) Hz, which is consistent with the above voltmeter measurement.

The experimental result and its uncertainty is plotted with the previously derived theoretical result in the one-dimensional graph in Figure 18. The percent difference between the experimental and theoretical values is 5%, whereas the maximum error bar is $\pm$ 0.5%, which is smaller an order of magnitude. Figure 18 thus clearly shows that the theoretical and experimental values do not agree within experimental error, especially because the error bars represent the worst-case uncertainty.

Figure 18. Comparison of theoretical and experimental resonance frequencies for a neckless spherical Helmholtz resonator

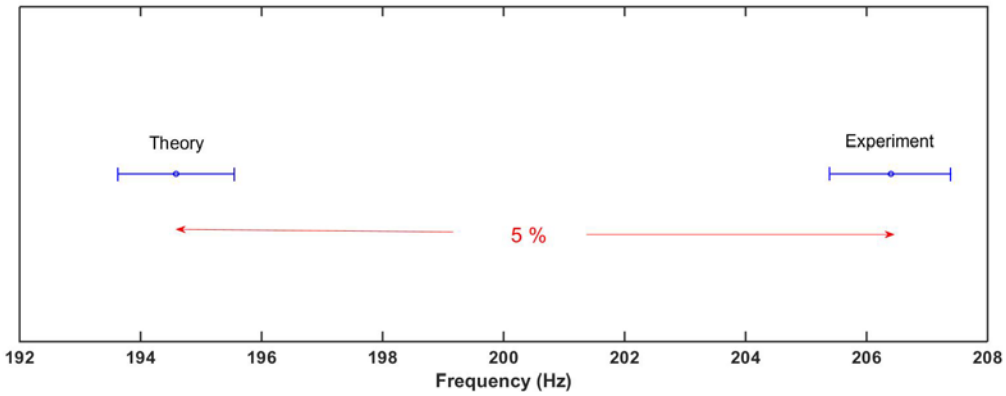

Comparison of theoretical and experimental resonance frequencies for a neckless spherical Helmholtz resonator. The error bars represent a worst-case analysis.

There are several possible reasons for the experimental frequency being significantly greater and theoretical value. For a neckless Helmholtz resonator, the flow of air at the orifice is expected to increasingly diverge as the distance from the axis increases, whereas the theory assumes that the fluid acts as a piston. The actual flow would then exhibit less inertia, which would cause the experimental frequency to be *greater* than the theoretical frequency. This is what we observe.

Another possible reason for the discrepancy is due to the fact that the orifice does not have an infinite planar flange, which is assumed in the theory. Our flange is finite and curved. This geometry would lower the inertia on the outside because the flow has greater divergence. Inside, however, the curvature causes the inertia to increase. The two effects thus compete. To our knowledge, it is not known whether the net effect is an increase or decrease in frequency.

To attempt to resolve the extent to which the piston assumption is responsible for the theoretical frequency being less than the experimental frequency, we performed an experiment with a precision cylindrical Helmholtz

resonator that has a relatively large planar flange. This is the subject of the next two sections.

E. CYLINDRICAL SHELL THEORY

Our development in this section parallels that in Section C for the theoretical resonance frequency of a spherical Helmholtz resonator. Figure 19 displays the applicable physical dimensions for determining the resonance frequency of a flanged cylindrical Helmholtz resonator with a circular opening. The resonance frequency is calculated by Eq. (1) where c is the speed of sound in air, $S = \pi R^2$ is the surface area, $V = \pi R^2 h$ is the volume of the cylinder, and the effective length of the neck is given by Eq. (2) for a theoretically assumed piston of air mass oscillating in the opening of the cylinder.

Figure 19. Geometry of a flanged cylindrical Helmholtz resonator with a circular opening

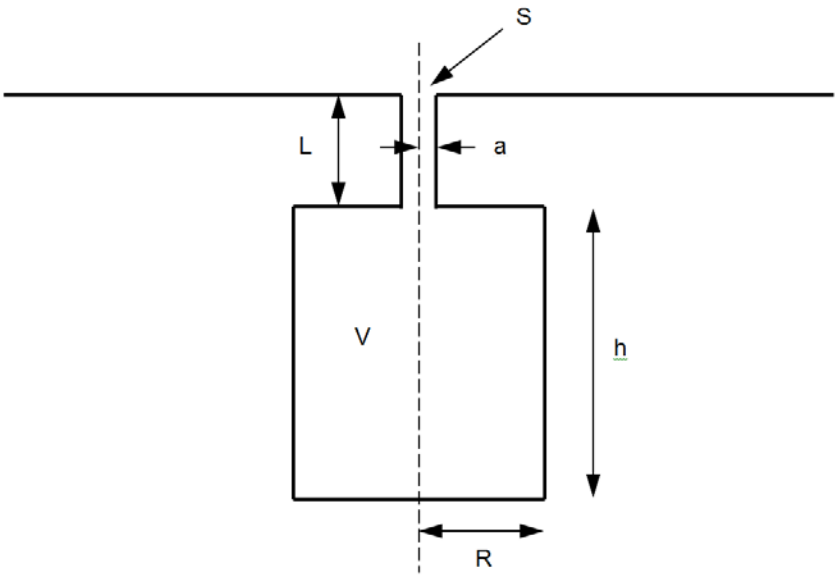

Accurate measurements of the dimensions and the temperature at which the experiment was performed are:

$$2R = (7.987 \pm 0.0095)\,\text{in}$$

$$2a = (0.503 \pm 0.0015)\,\text{in}$$

$$L = (0.0405 \pm 0.001)\,\text{in} \qquad h = (9.899 \pm 0.003)\,\text{in}$$

$$T = (24.6 \pm 0.3)\,^{\circ}\text{C}$$

The values of relevant geometrical parameters are

$$S = \pi a^2 = \pi\left(\frac{0.503}{2}\,\text{in}\right)^2 = 0.199\,\text{in}^2,$$

$$V = \pi R^2 h = \pi\left(\frac{7.987}{2}\,\text{in}\right)^2 (9.899\,\text{in}) = 496.0\,\text{in}^3,$$

$$L_{\text{eff}} = 0.0405\,\text{in} + 1.70\left(\frac{0.503}{2}\,\text{in}\right) = 0.468\,\text{in}.$$

From the values of these quantities, and the speed of sound at room temperature T_0 = 293.15 K (20°C), we find that the theoretical resonance frequency is

$$f_{\text{room}} = \frac{c}{2\pi}\sqrt{\frac{S}{L_{\text{eff}} V}} = \frac{\left(343.2\frac{\text{m}}{\text{s}}\right)\left(39.37\frac{\text{in}}{\text{m}}\right)}{2\pi}\sqrt{\frac{0.199\,\text{in}^2}{(0.468\,\text{in})(496.0\,\text{in}^3)}} = 63.0\,\text{Hz}$$

As in the previous spherical Helmholtz resonator case, to determine the theoretical value of the resonance frequency for the experiment, we simply scale the 63.0 Hz value by $(T/T_0)^{1/2}$, where T is the average absolute temperature during the experiment.

The result for the theoretical resonance frequency is then

$$f = \sqrt{\frac{T}{T_0}}\, f_{\text{room}} = \sqrt{\frac{297.75}{293.15}}\, 63.0 = 63.5\,\text{Hz}.$$

Similar to the case of the spherical Helmholtz resonator, we estimate the uncertainty of the cylindrical Helmholtz theoretical resonance frequency as follows. The resonance frequency (1) is

$$f = \frac{c}{2\pi}\sqrt{\frac{S}{L_{eff}V}} = \frac{c}{2\pi}\sqrt{\frac{\pi a^2}{(L+1.70a)\pi R^2 h}}.$$

Because the geometrical length L is small compared to the radius a, the frequency is approximately

$$f = \frac{c}{2\pi}\sqrt{\frac{\pi a^2}{(1.70a)\pi R^2 h}} = \frac{c}{2\pi}\sqrt{\frac{a}{(1.70)R^2 h}} = \frac{c}{2\pi}\left(\frac{1}{\sqrt{1.70}}\right)\frac{a^{1/2}}{Rh^{1/2}}.$$

Determining the fractional differential of f due to each of the fractional uncertainties $\delta a/a$, $\delta R/R$, $\delta h/h$, and $\delta c/c = \delta T/2T$, where T is the absolute temperature, and adding the results for a worst-case error analysis, yields

$$\frac{\delta f}{f} = \frac{\delta a}{2a} + \frac{\delta R}{R} + \frac{\delta h}{2h} + \frac{\delta T}{2T}.$$

Inputting the values and multiplying by the theoretical frequency, we find that the worst-case uncertainty of the theoretical resonance frequency is

$$\delta f = \pm(63.0\ \text{Hz})\left[\frac{0.0015}{2(0.503)} + \frac{0.0095}{7.987} + \frac{0.003}{2(9.899)} + \frac{0.3}{2(297.75)}\right]$$

$$= \pm(63.0\ \text{Hz})[0.0015 + 0.0012 + 0.00015 + 0.00050] = \pm 0.2\ \text{Hz}.$$

The uncertainty is ±0.3%. The final value of the theoretical resonance frequency of the cylindrical Helmholtz resonator is

$$f = (63.5 \pm 0.2)\ \text{Hz}.$$

In the next section, we determine an experimental value of the resonance frequency, and compare this value to the theoretical value.

F. CYLINDRICAL SHELL EXPERIMENT

Our cylindrical Helmholtz resonator is shown in Figure 20. The resonator consists of a 1/4-in thick clear acrylic tube with a height of approximately 10 in

and inner diameter 8 in (precise dimensions are stated in Section E). The tube is permanently adhered to a 3/8-in thick acrylic base plate. The top plate is 1/25-in thick steel plate that is screwed into the top of the cylindrical tube, so that the top plate could be changed. Vacuum grease was used to seal the top plate and the tube. The diameter of the concentric hole in the metal plate is 1/2 in. Note that this can be drilled out to successively larger diameters in the future if data needs to be collected for a range of hole diameters.

Figure 20. Experimental setup for determining resonance frequency of an approximately neckless cylindrical Helmholtz resonator

As shown in Figure 20, the experimental setup for the cylindrical Helmholtz resonator is similar to that in Section D for the spherical Helmholtz

resonator. We excite the Helmholtz mode with a JL Audio 5–1/2-in diameter 150-W subwoofer driven by a function generator and power amplifier. A 1/8-in threaded Endevco microphone 8510B-1 is fitted inside the cylinder and is connected to a conditioner box. The signal from the box is sent to a Stanford Research Systems preamplifier model SR560, which also serves as band pass filter. The drive frequency is adjusted on the function generator until the received voltage is maximized.

The experimental resonance frequency was surprisingly found to depend upon the amplitude of the loudspeaker, even though the maximum root-mean-square drive amplitude of 4 V was not loud to the ear at all. We experimented with the spherical Helmholtz resonator (Sections B, C, and D), as well as a PH3451 laboratory Helmholtz resonator, and observed *no* amplitude dependence of the resonance frequency.

To accurately quantify the amplitude dependence, we used a lock-in amplifier (Stanford Research Systems model 560) in the synchronous (< 200 Hz) mode with a 1.0 s time constant and a 24 dB/octave filter roll-off. Pre-filtering and gain were accomplished with preamplifier (Stanford Research Systems model SR560). We were able to readily quarter the error bars compared to the previous readings from a multimeter. Figure 21 shows a graph of the experimental resonance frequencies and their uncertainties as a function of the root-mean-square drive voltage across the loudspeaker. The theoretical frequency from Sec. E is plotted as a solid constant line with dashed constant lines denoting the uncertainty. The minimum drive amplitude of 0.125 corresponds to barely audible sound.

Figure 21. Cylindrical Helmholtz resonator (Normal Incidence)

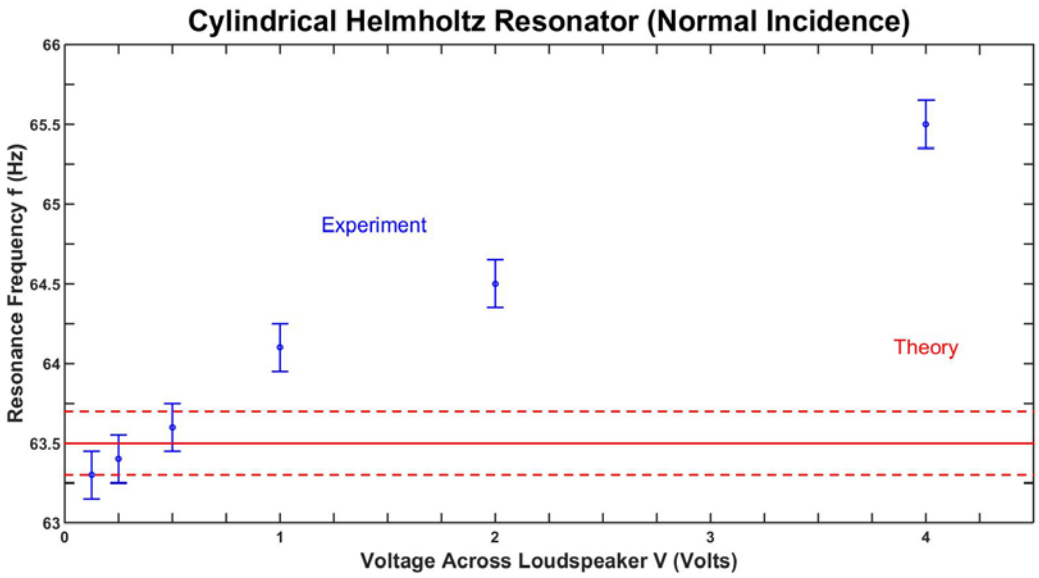

Resonance frequency as a function of loudspeaker drive amplitude for a neckless cylindrical Helmholtz resonator. The error bars represent a worst-case analysis. The theoretical resonance frequency is constant with respect to drive voltage.

The graph in Figure 21 clearly shows that the resonance frequency increases with amplitude. The effect may be due to the thinness of the neck (0.0405 in), which is roughly half the value of the neck of the spherical resonator (0.069 in). If this is the case, there could be a dependence on the angle of incidence of the sound wave from the loudspeaker, as a result of the velocity of the sound wave. However, data gathered for grazing and normal incidence agree well within the error bars.

The fact that the experimental resonance frequency at low amplitude agrees with the theoretical value strongly supports the validity of the piston assumption in the derivation of the end correction. The problem is then to understand why there is a significant systematic error in the case of the spherical Helmholtz resonator (Section D). The only apparent possibility is that the curvature of the baffle is responsible. This is surprising because, in regard to the resonance frequency, the curvature has opposite (competing) effects inside and

outside the opening (refer to Section D). More research needs to be done to confirm this effect.

A possible way to account of the observation of an amplitude-dependent resonance frequency in the cylindrical resonator is as follows. Sufficiently large amplitudes of a Helmholtz resonator lead to turbulence at the opening. Helmholtz resonators with a sufficiently small neck length are expected to develop turbulence at smaller amplitudes. Because the turbulence increases with amplitude, we expect the quality factor to decrease with amplitude. If, in addition, the drive amplitude is not constant in the vicinity of the resonance, the resonance frequency will change with amplitude. Specifically, if the drive amplitude increases in the vicinity of the resonance, the resonance frequency will increase with amplitude.

In the case of the cylindrical resonator, we checked the drive amplitude of the loudspeaker by completely covering the hole of the resonator with a metal plate. We indeed observed a weak increase in drive amplitude in the vicinity of the resonance. In the absence of the spherical Helmholtz resonator, the drive amplitude in the vicinity of the resonance was observed to be nearly constant.

We did not have the time to quantitatively investigate the hypothesis of the combination of an amplitude-dependent quality factor and a nonconstant drive amplitude causing the amplitude-dependence of a Helmholtz resonance frequency. This topic is for future work.

G. CONCLUSIONS AND FUTURE WORK

Helmholtz resonators are very common, occurring in a wide variety of systems. These resonances are often intended, but are sometimes unintentional and unwanted. An important special case is a “neckless” Helmholtz resonator, where the geometrical neck length is small compared to the characteristic size of the opening (the diameter for a circular opening). In this case, the calculation of the inertia strongly involves the end correction for pipe. If this effect is not

included, the theoretical frequency of the resonance will be much greater than the actual frequency.

We have shown that a simple but effective lecture demonstration of a neckless Helmholtz resonator is thin plastic 6-in diameter sphere with a 1-in diameter hole in it. The resonance is excited by blowing across the hole by mouth, and the sound can be clearly heard. The measured frequency is about 200 Hz, while the predicted frequency without the end correction is about 700 Hz, which is dramatically different. Including the end correction yields about 190 Hz, which is much closer to the observed frequency.

However, a careful experimental and theoretical analysis with the spherical neckless Helmholtz resonator reveals that the experimental and theoretical values do *not* agree within experimental error. The experimental value is greater by 5%, while the worst-case error bars are less by an order of magnitude. We had suspected that this might occur, because the end correction is based on the assumption that the flow near the opening acts as a piston. While this may be a good approximation for a nonneckless Helmholtz resonator, it could yield an overestimate of the end correction for the neckless case due to an expected strong divergence of the flow. However, the discrepancy could instead be due to the curvature of the sphere, because the theory assumes an infinite planar baffle.

To attempt to resolve what is responsible for the deviation of the experimental and theoretical values, we performed a theoretical and experimental analysis of a precision cylindrical Helmholtz resonator with a planar baffle that is large compared to the hole diameter. For small amplitudes, agreement between theory and experiment occurs, which strongly suggests that the piston assumption is valid. However, two other issues arose.

First, if the piston assumption is indeed valid, then the discrepancy of the experimental and theoretical resonance frequencies of the spherical resonator

would appear to be due to the lack of a large planar baffle. A future topic of research is to investigate this possible effect.

Second, why does the cylindrical resonator have an amplitude-dependent resonance frequency for the low amplitudes of the experiment? As qualitatively explained in Section F, we suspect that this is due to a combination of two effects. One is a decreasing quality factor Q as the amplitude is increased, which could be due to the ease with which turbulence is expected to occur for a neckless resonator. The other is an increasing acoustic drive amplitude, which was observed to weakly occur. Future topics of research include mathematically checking a driven damped harmonic oscillator with the combination of Q that decreases with amplitude and a drive amplitude that increases as the frequency is varied. According to our qualitative arguments, the resonance frequency should increase with overall amplitude. In addition, an experiment should be conducted such that the acoustic drive amplitude is arranged to be constant, which should yield *no* amplitude dependence of the resonance frequency. The quality factor as a function of amplitude should also be experimentally explored.

In regard to the cylindrical resonator, the compliance of the top is expected to cause an amplitude-independent lowering of the resonance frequency. We forgot to check for this effect, which can be done by touching the top with one or more finger tips.

THIS PAGE INTENTIONALLY LEFT BLANK

V. OVERALL CONCLUSIONS AND FUTURE WORK

A. CONCLUSIONS

We have investigated new physics lecture demonstrations in three areas that are important in the Undersea Warfare curriculum: reciprocity in linear passive electrical networks, a Cartesian diver including buoyancy, and neckless Helmholtz resonators.

Reciprocity has a number of important uses in underwater acoustics, including the existence of equivalent electric circuits for most sonar transducers. In our investigations of linear passive electrical networks, we showed that an existing large 2-dimensional resistor grid can serve as a lecture demonstration of reciprocity. We also showed that the small error in reciprocity is due to the shunt resistance of the current meter which is used to measure the response. We also developed a two randomly generated networks of resistors, capacitors, and inductors, and very accurately verified reciprocity in both cases with the software PSpice.

Our Cartesian diver of an open inverted glass test tube offers three possible definitions of the body. One is appropriate for the explanation of the use of ballast tanks to cause a submarine to sink or rise. We have quantitatively confirmed that all three possible choices lead to the same condition for sinking. We have also shown that our Cartesian diver apparatus can be used to conclusively demonstrate that a neutrally-buoyant body is unstable. Surprisingly, a hydrostatic paradox occurs when the instability is attempted to be explained for the simplest case of a Cartesian diver in a perfectly rigid container where the water is assumed to be incompressible. We resolved the paradox by allowing the container to have a compliance. Finally, we theoretically showed that a neutrally-buoyant body cannot be parametrically stabilized by pressure modulations, but can be stabilized by modulations of the acceleration due to gravity.

Helmholtz resonators have been proposed as low-frequency sources of underwater sound, and can unintentionally occur on the surfaces of submarines. Neckless Helmholtz resonators, where the geometrical neck length is small compared to the acoustic end correction, often occur. We have shown that a thin plastic sphere with a hole serves well as a quantitative lecture demonstration. Comparison of the measured and predicted resonance frequencies shows that the end correction plays a critical role. In a careful experiment, we showed that the experimental and theoretical frequencies do not agree within experimental error. To resolve the source of the error, we performed an experiment with a precision cylindrical resonator, which showed agreement with theory but only at very low acoustic amplitudes. The reason may be partly due to the quality factor decreasing with amplitude due to turbulence generated by a thin orifice.

B. FUTURE WORK

Future work in reciprocity in electrical networks includes the construction and testing of the randomly generated network that is described in Sec. II.C. In addition, the subject of reciprocity in mechanical equilibrium systems offers several lecture demonstrations, one of which already is in use at NPS. However, careful data have not yet been taken. An interesting aspect of these demonstrations is that nonlinearity is expected to be present. It would be interesting to observe the expected breakdown of reciprocity due to nonlinearity.

Future work related to the Cartesian diver is to perform an experiment to attempt to stabilize a neutrally-buoyant diver. According to our theory, this could be accomplished by vertically oscillating the container (and thus effectively modulating the acceleration due to gravity). Attempts should also be made by modulating the pressure, because this would have a possible application of using underwater sound to stabilize small neutrally-buoyant probes in the ocean. Our theory predicts that this modulation cannot cause stabilization, but a number of approximations have been made in the theory. A successful experiment in the parametric stabilization should then be adapted as a lecture demonstration.

Future work with neckless Helmholtz resonators includes measurements of the quality factor as a function of amplitude. Our results indicate that the quality decreases quickly with amplitude, which may be due to the ease with which turbulence can occur for very thin necks.

THIS PAGE INTENTIONALLY LEFT BLANK

LIST OF REFERENCES

An, C., Alaie, S., Sovani, S., Scislowicz, M. (2004). Side window buffeting characteristics of an SUV, Society of Automotive Engineers (SAE) technical paper 2004-01-0230.

Arunajatesan, S. and Sinha, N. (2005, May). Modeling Approach for reducing Helmholtz resonance in submarine structures. Paper presented at the eleventh AIAA/CEAS Aeroacoustics Conference (Twenty sixth AIAA Aeroacoustics Conference), Monterey, California.

Atra, A. B., and Salleh, H. (2013, July). Simulation of acoustic energy harvester using Helmholtz resonator with piezoelectric backplate. Presented at the Twentieth International Congress on Sound and Vibration (ICSV20), Bangkok, Thailand.

Benade, A. H. (1990). *Fundamentals of musical acoustics*, 2nd ed. New York, Dover, 489–492.

Blanchfield, J., Garrett, C., Wild, P., Rowe, A. (2008). The extractable power from a channel linking a bay to the open ocean. *Proc. Institution of Mechanical Engineers, Part A: J. Power and Energy*, 222, 289–297.

Brandon, Ann (1982). A beautiful Cartesian diver. *Physics Teacher*, 20, 482–483.

Bruce C. Denardo, Joshua J. Puda, & Andrés Larraza (2009). A water wave analog of the Casimir effect. *American Journal of Physics,* 77, 1095–1101.

Butler, William A. (1981). Reverse Cartesian diver "trick." *American Journal of Physics*, 49, 92.

Carpenter, D. Rae (2003). Another diver/riser. *Physics Teacher*, 41, 133.

Couper, T. (2014, October 4). Helmholtz resonance might be driving you nuts. Retrieved from http://blogs.unimelb.edu.au/sciencecommunication /2014/10/04/helmholtz-resonance-might-be-driving-you-nuts/

Denardo, B. (2015). Lecture Notes and Problem Solutions for PH4454: Sonar transducer theory and design, Physics Department, Naval Postgraduate School, Ch. 2 and Problem Set 2.

Denardo, B., Earwood, J., & Sazonova, V. (1999). Experiments with electrical resistive networks, *American Journal of Physics*, *67*, 981–986.

Denardo, Bruce C.(2012). Nonlinear oscillations and waves: *An introduction with demonstrations (Lecture Notes and Problems for PH4459)*, Physics Department, Naval Postgraduate School, Ch. 3.

Dietz, Frank T. (1974). More on the Cartesian diver. *Physics Teacher*, 12, 61.

Emerson, S. (2015). Development of Physics lecture demonstrations, Master's thesis, Physics Department, Naval Postgraduate School.

Frazier, Richard (2015). A philosophical toy. http://courses.education.illinois.edu /CI241-science-Sp95/resources/philoToy/philoToy.html

Fakhruddin, Hasan (2003). Cartesian diver and riser, *Physics Teacher* 41, 53.

Fakhruddin, Hasan (2011). … And now a suspended Cartesian diver. *Physics Teacher*, 49, 58.

Fletcher, N. H., & Rossing, T. D. (2004). *The Physics of musical instruments*, 2nd edition. New York, Springer, Secs. 16.1–16.8. This book has a detailed and lengthy quantitative explanation of the excitation of flutes by a steadily impressed flow. The Helmholtz resonator is a member of the flute family.

Gillis, K. A., & Moldover, M. R. (2014). Acoustic techniques for measuring transport Properties of Gases in *Experimental Thermodynamics*, Vol. IX: *Advances in Transport Properties of Fluids*, pp. 1–18.

Glezer, A., & Amitay, M. (2002). Synthetic jets, Annu. Rev. Fluid Mech. **34**, 503–529.

Güémez, J., Fiolhais, C., & Fiolhais, M. (2003). A demonstration apparatus of the Cartesian diver. *Physics Teacher*, 41, 495–496.

Güémez, J., Fiolhais, C., & Fiolhais, M. (2002). The Cartesian diver and the fold catastrophe. *American Journal of Physics*. 70, 710–714.

Graham, Robert M. (1989). An extremely sensitive Cartesian diver. *Physics Teacher*, 32, 182–183.

He, Sheng-ping, Mak, Se-yuen, & Zhu, Eqing. (1993). Toys in teaching physics: Cartesian diver. American Journal of Physics, 61, 938–940.

Helmholtz, H. L. F. (1954). *On the sensations of tone.* New York, Dover, pp. 43–44, 51, 92, 372–474. Baron Herrmann Ludwig Ferdinand von Helmholtz (1821-1894) was a German physician, physicist, mathematician, and philosopher. His classic treatise includes a bewildering collection of theoretical and experimental formulas for what is now known as the Helmholtz resonance frequency. The collection is apparently due to the fact that the end corrections were not well-established at the time the book was written.

Honda Vehicle Model Information. (n.d.). Retrieved from http://owners.honda.com/vehicles/information/2006/Pilot/specs#mid^YF1846EW

Jenkins, Alejandro (2004). An elementary treatment of the reverse sprinkler. *American Journal of Physics*, 72, 1276–1282.

John W. M. Bush (2015). Pilot-wave hydrodynamics. *Annual Review of Fluid Mechanics*, 47, 269–292.

Jones, Robert N. (1973). The Cartesian diver. *Physics Teacher*, 11, 345.

Kinsler, L. E., Frey, A. R., Coppens, A. B., & Sanders, J. V. (2000). *Fundamentals of Acoustics*, 4th edition. New York: Wiley.

Kirkpatrick, Paul (1942). A neglected lesson from the Cartesian diver. American Journal of Physics. 10, 160.

Knollenberg, R. B., III (1989). An automated Cartesian diver apparatus. *Physics Teacher*, 27, 51.

Kotheimer, Richard F. (1974). Cartesian diver. *Physics Teacher*, 12, 576.

Kruglak, Haym (1975). The rising Cartesian diver. *Physics Teacher*, 13, 68–69.

Landau, L. D., and Lifshitz, E. M.(1976) *Mechanics*, 3rd edition. New York, Pergamon.

Lee, Edward V. (1981). Cartesian diver with pressure head. *Physics Teacher*, 19, 416.

Loverude, Michael E. (2009). A research-based interactive lecture demonstration on sinking and floating. *American Journal of Physics*, 77, 897–901.

Loverude, Michael E., Kautz, Christian H., and Heron, Paula R. (2003). Helping students develop an understanding of Archimedes' principle. I. Research on student understanding. *American Journal of Physics*, 71, 1178–1187.

Mackay, R. Stuart (1958). Automatic Cartesian diver. *American Journal of Physics*, 26, 403–404.

Miller, Julius Sumner (1954). Extensions of the Cartesian diver experiment. *American Journal of Physics*, 22, 235–236.

Muller, Eric (1996). Condiment diver. *Physics Teacher*, 34, 296.

Orwig, Lawrence P. (1980). Cartesian diver tricks. *American Journal of Physics*. 48, 320.

Physics Stack Exchange. (2014). Question on the hydrostatic paradox. Retrieved from http://physics.stackexchange.com/questions/98610/question-on-the-hydrostatic-paradox

Pinkerton, K. David (2001). Sink or swim: The Cartesian diver. *J. Chem. Educ*. 78, 200A–200B.

Rabinovich, A. B. (2009). Seiches and harbor oscillations, in Kim, Y. C., ed., *Handbook of Coastal and Ocean Engineering.* Singapore, World Scientific, ch. 9.

Ragsdale, Terry (1989). Cartesian diver. *Physics Teacher*, 27, 306.

Rockwell, K. (2011). Zoom H4n Review. Retrieved from http://www.kenrockwell.com/audio/zoom/h4n.htm

Rossing, T. D., & Fletcher, N. H. (2004). *Principles of vibration and sound.* New York, Springer.

Rossing, T. D., ed. (2007). *Springer handbook of acoustics.* New York, Springer.

SAE International (2001, February 1). Surface vehicle recommended practices. Retrieved from https://law.resource.org/pub /us/cfr/ibr/005/sae.j1100.2001.html

STEM Careers in America's Navy. (n.d.). Retrieved from http://www.navy.com/stem.

Turner, Raymond C. (1983). Toys in teaching physics: Cartesian diver. *American Journal of Physics*, 51, 475–476.

Vladimirescu, A. (2015). *The spice book*. New York: Wiley.

Wild, R. L. (1981). Ultimate Cartesian diver set. *American Journal of Physics*. 49, 1185.

Wilson, O. B. (1989). *Introduction to the theory and design of sonar transducers.* Los Altos, California: Peninsula Publishing.

THIS PAGE INTENTIONALLY LEFT BLANK

INITIAL DISTRIBUTION LIST

1. Defense Technical Information Center
   Ft. Belvoir, Virginia

2. Dudley Knox Library
   Naval Postgraduate School
   Monterey, California